Defense Nuclear Agency
Alexandria, VA 22310-3398

DNA-TR-89-266

Diode Code Development

Nino Pereira
Ernest Alcaraz
Berkeley Research Associates, Inc.
P.O. Box 241
Berkeley, CA 94701

October 1990

Technical Report

CONTRACT No. DNA 001-84-C-0015

Destroy this report when it is no longer needed. Do not return to sender.

PLEASE NOTIFY THE DEFENSE NUCLEAR AGENCY, ATTN: CSTI, 6801 TELEGRAPH ROAD, ALEXANDRIA, VA 22310-3398, IF YOUR ADDRESS IS INCORRECT, IF YOU WISH IT DELETED FROM THE DISTRIBUTION LIST, OR IF THE ADDRESSEE IS NO LONGER EMPLOYED BY YOUR ORGANIZATION.

DISTRIBUTION LIST UPDATE

This mailer is provided to enable DNA to maintain current distribution lists for reports. We would appreciate your providing the requested information.

NOTE:
Please return the mailing label from the document so that any additions, changes, corrections or deletions can be made more easily.

- ☐ Add the individual listed to your distribution list.
- ☐ Delete the cited organization/individual.
- ☐ Change of address.

NAME: _____

ORGANIZATION: _____

OLD ADDRESS	CURRENT ADDRESS
_____	_____
_____	_____
_____	_____

TELEPHONE NUMBER: ( ) _____

SUBJECT AREA(s) OF INTEREST:

_____ _____

_____ _____

_____ _____

DNA OR OTHER GOVERNMENT CONTRACT NUMBER _____

CERTIFICATION OF NEED-TO-KNOW BY GOVERNMENT SPONSOR (if other than DNA)

SPONSORING ORGANIZATION: _____

CONTRACTING OFFICER OR REPRESENTATIVE _____

SIGNATURE _____

CUT HERE AND RETURN

Director
Defense Nuclear Agency
ATTN: TITL
Washington, DC 20305-1000

Director
Defense Nuclear Agency
ATTN: TITL
Washington, DC 20305-1000

REPORT DOCUMENTATION PAGE

Form Approved
OMB No. 0704-0188

1 AGENCY USE ONLY *(Leave blank)*	2. REPORT DATE	3. REPORT TYPE AND DATES COVERED
	901001	Technical 831011 to 860131

4 TITLE AND SUBTITLE

Diode Code Development

5 FUNDING NUMBERS

C - DNA 001-84-C-0015
PE - 62715H
PR - G37TMXG
TA - E
WU - DH007893

6 AUTHOR(S)

Nino Pereira and Ernest Alcaraz

7 PERFORMING ORGANIZATION NAME(S) AND ADDRESS(ES)

Berkeley Research Associates, Inc.
P.O. Box 241
Berkeley, CA 94701

8 PERFORMING ORGANIZATION REPORT NUMBER

BRA-90-W012R

9 SPONSORING MONITORING AGENCY NAME(S) AND ADDRESS(ES)

Defense Nuclear Agency
6801 Telegraph Road
Alexandria, VA 22310-3398
RAEV/Hebert

10 SPONSORING MONITORING AGENCY REPORT NUMBER

DNA-TR-89-266

11 SUPPLEMENTARY NOTES

This work was sponsored by the Defense Nuclear Agency under RDT&E RMSS Code B3230844662 G37TMXGE00016 H2590D.

12a DISTRIBUTION/AVAILABILITY STATEMENT

Approved for public release; distribution is unlimited.

12b DISTRIBUTION CODE

13 ABSTRACT *(Maximum 200 words)*

This final report, covering the work done under contract DNA 001-84-C-0015 during the performance period of 11 October 1983 to 31 January 1986, describes our research conducted in close coordination with the efforts at the Naval Research Laboratory. During this collaboration, we used and modified codes such as MAGIC, developed by Mission Research Corporation, to model vacuum diode regions of the DNA superpower ten terawatt generators such as the DNA/Aurora 14 TW pulser at the Harry Diamond Laboratories.

In regards to the unpredictable destruction of the tantalum anode during shots, it is shown that when ions are present in the diode gap, the electron flow pinches, resulting in a high energy density at the anode. This is believed to be a mechanism of the anode destruction. When ions are not present, our models show that the flow does not pinch. In coupling of the MAGIC code to a model of a Plasma Radiation Source it was also found that the electron flow outside of the pinch is much less important than anticipated with the maximum current in free electrons only a few percent of that through the pinch for typical plasma radiation sources as those used on multi-terawatt generators.

14 SUBJECT TERMS

Diode
Z-Pinch
X-Ray Sources
Plasma Radiative Source
Collisional Radiative Plasmas

15 NUMBER OF PAGES

66

16 PRICE CODE

17 SECURITY CLASSIFICATION OF REPORT	18 SECURITY CLASSIFICATION OF THIS PAGE	19 SECURITY CLASSIFICATION OF ABSTRACT	20 LIMITATION OF ABSTRACT
UNCLASSIFIED	UNCLASSIFIED	UNCLASSIFIED	SAR

CLASSIFIED BY

N/A since Unclassified.

DECLASSIFY ON

N/A since Unclassified.

CONVERSION TABLE

Conversion factors for U.S. customary to metric (SI) units of measurement.

To convert from	to	Multiply by
angstrom	meters (m)	$1.000\ 000 \times 10^{-10}$
atmosphere (normal)	kilo pascal (kPa)	$1.013\ 25 \times 10^{+2}$
bar	kilo pascal (kPa)	$1.000\ 000 \times 10^{+2}$
barn	meter^2 (m^2)	$1.000\ 000 \times 10^{-28}$
British thermal unit (thermochemical)	joule (J)	$1.054\ 350 \times 10^{+3}$
cal (thermochemical)/ cm^2	mega joule/m^2 (MJ/m^2)	$4.184\ 000 \times 10^{-2}$
calorie (thermochemical)	joule (J)	$4.184\ 000 \times 10^{+3}$
curie	giga becquerel (GBq)	$3.700\ 000 \times 10^{+1}$
degree Celsius	degree kelvin (K)	$t_K = t°_C + 273.15$
degree (angle)	radian (rad)	$1.745\ 329 \times 10^{-2}$
degree Fahrenheit	degree kelvin (K)	$t_K = (t°_F + 459.67)/1.8$
electron volt	joule (J)	$1.602\ 19 \times 10^{-19}$
erg	joule (J)	$1.000\ 000 \times 10^{-7}$
erg/second	watt(W)	$1.000\ 000 \times 10^{-7}$
foot	meter (m)	$3.048\ 000 \times 10^{-1}$
foot-pound-force	joule (J)	1.355 818
gallon (U.S.liquid)	meter^3 (m^3)	$3.785\ 412 \times 10^{-3}$
Gauss	Tesla	$1.000\ 000 \times 10^{-4}$
inch	meter (m)	$2.540\ 000 \times 10^{-2}$
joule/kilogram (J/kg) (radiation dose absorbed)	gray (Gy)	1.000 000
kilotons	terajoules	4.183
kip (1000 1 bf)	newton (N)	$4.448\ 222 \times 10^{+3}$
kip/inch^2 (ksi)	kilo pascal (kPa)	$6.894\ 757 \times 10^{+3}$
ktap	newton-second/m^2 (N-s/m^2)	$1.000\ 000 \times 10^{+2}$
micron	meter (m)	$1.000\ 000 \times 10^{-6}$
mil	meter (m)	$2.540\ 000 \times 10^{-5}$
mile (international)	meter (m)	$1.609\ 344 \times 10^{+3}$
ounce	kilogram (kg)	$2.834\ 952 \times 10^{-2}$
pound-force (1bf avoirdupois)	newton (N)	4.448 222
pound-force inch	newton-meter (N-m)	$1.129\ 848 \times 10^{-1}$
pound-force/inch	newton/meter (N/m)	$1.751\ 268 \times 10^{+2}$
pound-force/foot^2	kilo pascal (kPa)	$4.788\ 026 \times 10^{-2}$
pound-force/inch^2 (psi)	kilo pascal (kPa)	6.894 757
pound-mass (1bm avoirdupois)	kilogram (kg)	$4.535\ 924 \times 10^{-1}$
pound-mass-foot^2 (moment of inertia)	kilogram-meter^2($kg{\cdot}m^2$)	$4.214\ 011 \times 10^{-2}$
rad (radiation dose absorbed)	gray (Gy)	$1.000\ 000 \times 10^{-2}$
roentgen	coulomb/kilogram (C/kg)	$2.579\ 760 \times 10^{-4}$
shake	second (s)	1.000×10^{-8}
slug	kilogram (kg)	$1,459\ 390 \times 10^{+1}$
torr (mm Hg, O° C)	kilo pascal (kPa)	$1.333\ 22 \times 10^{-1}$

TABLE OF CONTENTS

LIST OF ILLUSTRATIONS

SECTION 1

INTRODUCTION

This final report, covering the work done under contract DNA001-84-C-0015 during the performance period from 11 OCT 83 to 31 JAN 86, describes the results of research conducted. The first task in the contract is to develop an appropriate electromagnetic, fully relativistic particle in cell code which realistically models the vacuum regions of the DNA superpower ten terawatt generators. Sections 2, 3 and 4 address this question.

One superpower generator is the DNA/Aurora pulser at the Harry Diamond Laboratories. Section 2 describes a diode which is modelled using a modified version of Mission Research Corporation's MAGIC code. It turns out that this code, written for this type of problem over the last few years under DOE sponsorship through Sandia National Laboratories, is able to handle the Aurora diode. The necessary modifications are in the code diagnostics, which are insufficiently flexible for our purpose. It is shown that without ions in the diode, the electron flow does not pinch as expected, while with ions the flow pinches, possibly resulting in destruction of the tantalum anode.

A conclusion from this work is that necessary PIC codes can evolve on the basis of existing codes. Such codes include MAGIC from MRC, C-CUBE (or ISIS) at Los Alamos National Laboratories, MASK at SAI, and others. For all the PIC code work under this contract we have used MAGIC.

An integral part of the statement of work is to combine the PIC code with other codes that are used by the DNA community, including z-pinch codes. Section 3 describes a modification to MAGIC that couples the code to a model of a Plasma Radiation Source. This research showed that the electron flow outside the pinch is much less important than anticipated. For a plasma radiation source typical of the ones used on multi-terawatt generators the maximum current in free electrons is only a few percent of the current through the pinch (for the parameters selected), and the maximum occurs in the early stage of the pinch, before peak radiation production. This work is described in Section 4.

We have also used the MAGIC code on bremsstrahlung diodes with low inductance. These diodes turn out to be exceedingly difficult to model. The reason is the widely disparate spatial and temporal scales that occurs simultaneously in such a diode. Under these circumstances it is impossible to find approximations that are valid uniformly throughout the diode region. Without approximations, however, a full computation would require excessive amounts of computational resources. A PIC computation on megavolt diodes with less than $\sim 1\ \Omega$ impedance remains an important problem to solve. Sustained research is needed to resolve this problem.

Task 2 is to continue the support of the NRL Advanced Concepts Theory program by providing atomic physics and chemistry models for plasma radiation sources. Sections 5 and 6 describe the efforts done under this task. Out of the research of leakage electron flow grew Section 5. Here, it is suggested that some alternate load configurations, that could be expected to enhance the desired x-ray output from a plasma radiation source, be tried.

Our background in collisionless plasma physics suggested that we evaluate the need to consider imperfectly collisional radiative plasmas. Section 6 contains our estimates. This work shows that the hot spots in plasma radiation sources, which are responsible for much of the harder x-rays, may be partly powered by non-maxwellian electrons that preferentially excite higher atomic energy levels than are accessible by a thermal, maxwellian distribution. In follow-on work it will be necessary to evaluate this phenomenon in more detail.

Task 3 covers the transfer of working versions of the codes developed under this contract to DNA, and to provide user guides to go with the codes. All codes and modifications to codes are available at NRL. Section 2 contains a sample of code input, and Section 3 includes a sample of a modification to the MAGIC code. The comments throughout are sufficent to guide others to reproduce our work, and to use it in their research. The code developed for Section 4, the Fokker-Planck code FOKKER, is available at NRL.

SECTION 2

AURORA DIODE SIMULATIONS

2.1 INTRODUCTION.

Every once in a while the anode in the Aurora flash x-ray simulator sustains damage, necessitating replacement of the converter foil at a considerable expense in downtime of the machine. The erratic occurrence of anode damage shows that there is no obvious cause for the damage. Theoretical, numerical and experimental studies of anode damage on much lower impedance machines such as Gamble II at the Naval Research Laboratory prove that ion emission followed by plasma emission from the anode neutralizes the electric charge in the electron beam, after which magnetic pinching takes over. Damage occurs when the localized energy deposition exceeds what is needed for melting or evaporization.

The numerical simulations described in this report suggest that also in Aurora the anode damage is connected with ion emission from the anode. Without ion emission, the electron beam hits the anode in a ring with approximately the cathode radius; when emission of protons is included the electrons pinch down to the center of the anode, and remain concentrated there until the end of the pulse. Pinching occurs only after the ions have reached the cathode, and charge neutralisation has taken place in the diode's center.

Pinching in the simulations is of course not erratic, in contrast to the experience at Aurora. Hence the simulations do not explain the anode damage, although they were done toward this purpose; other mechanisms must be invoked, e.g. varying amounts of background gas and anode surface phenomena. However, diode modeling of Aurora's diodes has not previously been done, and the results here are interesting in their own right for what they predict about the x-ray pulse. Namely, the simulations suggest that the x-ray pattern should be ring-shaped during the first 40 ns, but afterwards the ring collapses on axis leading to an intense central spot in the later part of the pulse.

Time-integrated measurements are consistent with these results, however time-resolved measurements are not yet available. The 10 ns x-ray risetime of the central x-ray pulse suggested by the computations may motivate such measurements. Differences between the measured data and the simulations should give further information on additional phenomena left out of the simulations, such as the influence from slowly ionizing background gas.

2.2 SIMULATIONS.

The 2-1/2 dimensional electromagnetic particle code MAGIC used in the simulations allows a non-uniform grid shown in Fig. 1. Only the front end of the diode is represented. The diode is 1 meter long and has a radius of 60 cm. Electron emission is allowed from the shank starting at 20 cm into the diode, and from the tip and inside of the cathode. In the run to be discussed ions are emitted from the center part of the anode. Other runs had different parameters for electron and/or ion emission, and various grid sizes, without appreciable change in the results. Section 2.4 contains the input for the run under discussion.

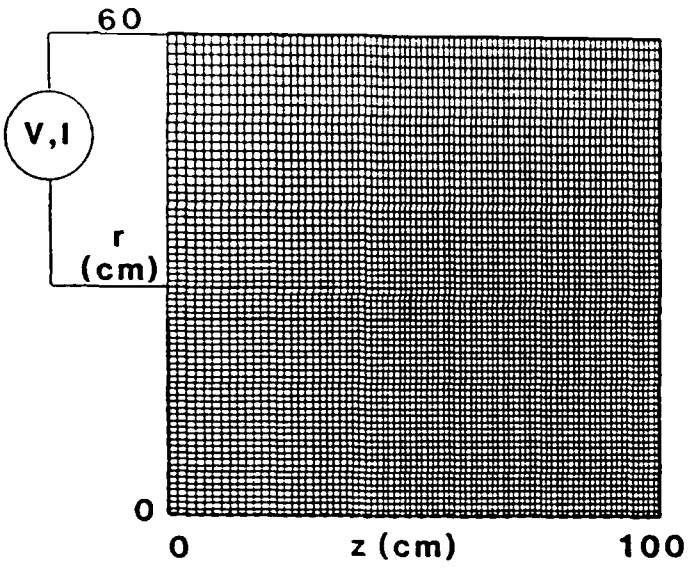

Figure 1. Diode geometry including hollow ring cathode, flat anode, and location of the voltage and current monitors at diode entrance. The grid is nonuniform, decreasing from the top inlet to the center anode by a factor of 2.

The voltage in Fig. 2 is close to a typical Aurora voltage, perhaps slightly shorter. The dashed line in Fig. 2 is the magnetic field B_θ at the outer edge (0.60 m) of the diode, or the current as determined from $I(MA) = 5B_\theta r$, where $B_\theta(T)$ and $r(m)$ are in MKS units. The voltage and current track each other very well, indicating a constant impedance of 37 Ohm in agreement with experience. It may seem surprising that the impedance remains almost constant, even though the dynamics of ions and electrons in the gap changes considerably during the pulse, see below. The reason is that much of the current is carried by the electron sheath

outside the cathode, where the balance between electric and magnetic fields remains unchanged since no ions make it to the outside of the cathode.

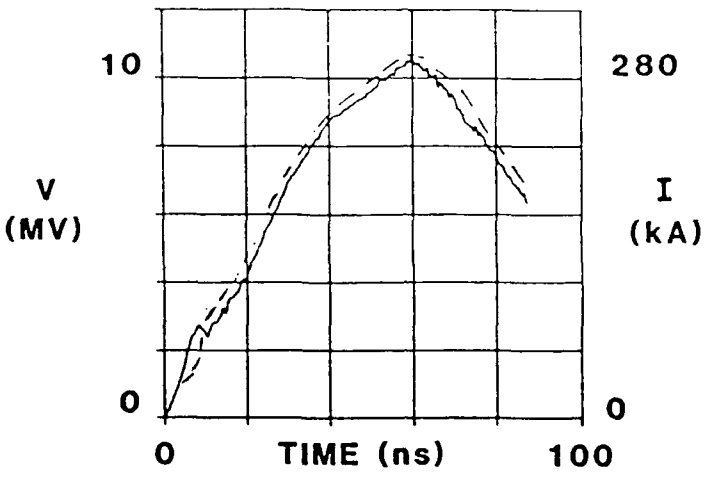

Figure 2. Voltage (solid) and current (dashed) at the diode inlet.

Pinching of the electron beam occurs at around 40 ns. Before the beam pinches the electrons move as in Fig. 3, at 37.5 ns. The electrons come off the shank and form a space charge sheath with an edge that after a small transition region becomes roughly parallel to the cathode. Electron emission from the shank is not quite uniform, but this is a feature of the threshold field in the emission algorithm. Emission off the tip of the cathode is uniform, but the electrons come off in bunches that propagate directly to the anode. The electron bunches reflect the emission parameters: electrons are emitted only after electric field has had a chance to build up. From the constant interbunch distance in these electrons it is evident that they move at the light speed. It takes the electrons about 3 ns to traverse the diode gap.

The ions (protons) are shown in Fig. 4 at the same time. At this time the ions have not yet reached the cathode. They cross the diode gap rather uniformly, perhaps partly attracted by the electron beam. The ions are denser near the anode because they are emitted with a small velocity, hence they need some time to accelerate into the gap.

Ion emission in the simulations is not quite realistic. While field emission for the electrons is well-established, including the space-charge limit coming from the

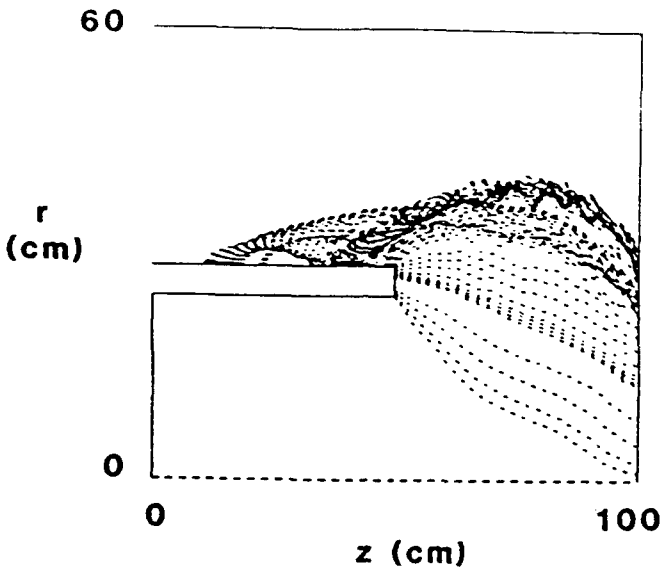

Figure 3. Electron trajectories before pinching, at 37.5 ns.

condition that the normal electric field vanish at the conductor surface, ion emission is not standard. The code uses the same algorithm for both electrons and ions, and the result is that the ions are emitted almost simultaneously with the electrons, once the electric field has exceeded 200 kV/cm. To represent the suspicion that ions are only emitted once the electrons have heated up the anode surface the ion emission is restricted here to the center part of the anode, somewhat arbitrarily bounded by the impact radius of the electrons at the time shown in Fig. 3, ie. 37.5 ns.

Electron and ion phase space (p^z vs z) in Figs. 5 and 6 corroborate the laminar development of the electron and ion streams. The electron phase space, Fig. 5, shows the space charge sheath on the cathode's outside, between 10 and 40 cm. Electrons there have traversed part of the potential difference, about 1 MeV, and are magnetically insulated. Once they get to the cathode edge the electrons pick up energy as they move toward the anode. Ion phase space is simple: each ion behaves almost the same, simply accelerating in the applied potential, with a slight variation in energy related to the radial motion.

A short 12.5 ns later, at 50 ns, the electrons pinch as shown in Fig. 7. The space charge sheath on the cathode is little modified, but as the electrons pass the cathode tip they move radially inward toward a point in front of the anode center. Their motion in this region is not properly represented in the simulation because the grid size in this highly complicated region appears insufficient to resolve the fields

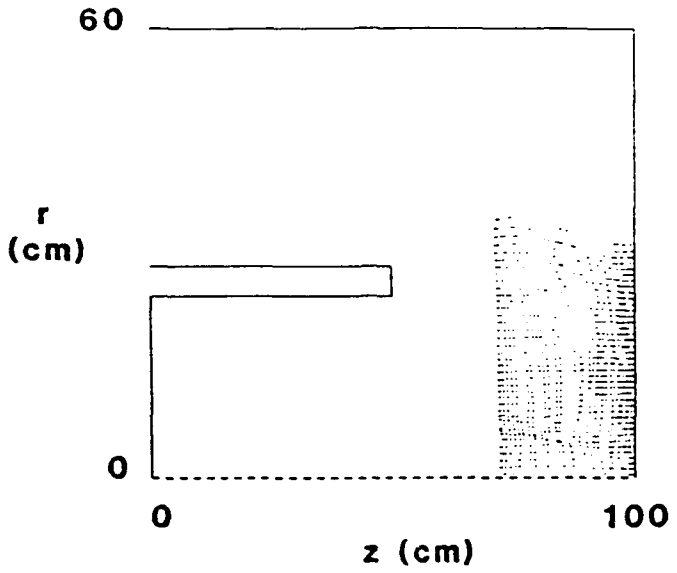

Figure 4. Ion trajectories before pinching, at 37.5 ns.

properly: the pinching coincides with the appearance of some noise on voltage and current (less than 5 %: suppressed in Fig. 2) and the onset of a loss in total energy (up to 6 %). Thus the details in the pinch region are suspect, and will not be quoted. However, the development toward the pinch phase is properly computed and should be realistic. There are also a few electrons inside the cathode moving away from the anode.

Ion trajectories in Fig. 8 are clustered about the electron beam, with continuing ion motion toward the inside of the cathode and some ions reaching the outside of the cathode tip.

As seen in Fig. 9, the electron phase space (p_z vs z) still contains the same space charge sheath as 12.5 ns earlier, but 20 cm from the anode many electrons lose their forward momentum, partly to be regained closer to the anode. However, much of the electron energy now resides in radial electron motion. In addition, some electrons are going backwards toward the inside of the cathode.

The ions inside the cathode still move in a laminar fashion, viz. the ion phase space in Fig. 10, but close to the pinch the ions are accelerated beyond the diode voltage, apparently due to strong electric fields local to the pinch region. Such details will have to be corroborated by better resolution in the pinch region. However, it is clear that the ions are oscillating about the electron beam, partly neutralizing its space charge and allowing the pinching to occur.

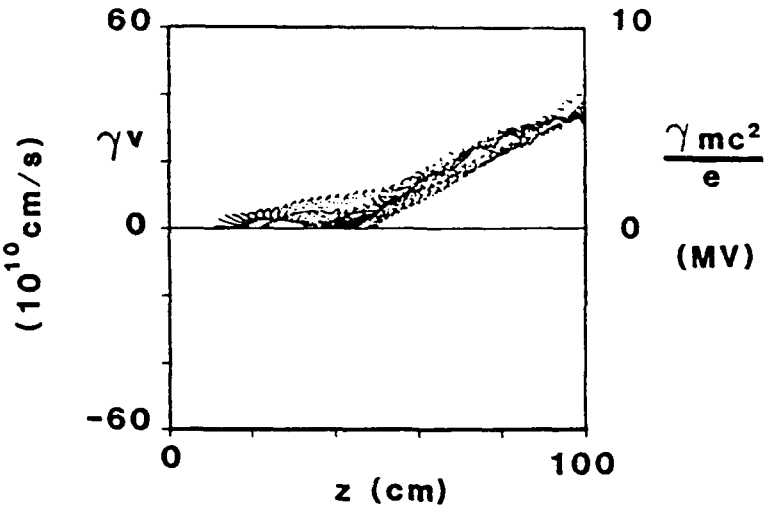

Figure 5. Electron phase space: axial momentum p_z versus axial distance z, at 37.5 ns.

Evidently there are many differences between reality and the simulation, and some of these will be metioned. How ions are introduced into the code appears particularly important. The code assumes that ions are emitted whenever the electric field exceeds a particular value (here $2 \times 10^7 V/m$). While this may be reasonable for the field-emitted electrons in reality the ions are thought to be emitted when the surface has gotten hot from electron bombardment followed by outgassing, or some similar mechanism. In any case there is probably a time delay in the ion emission that has not been properly represented in the computation. A code modification is necessary to represent this feature.

The ionic species may also be important. The computation assumes a single species, singly charged hydrogen. In reality there may be a mixture of H^+, C^+ and/or C^{++}, and probably other ions as well. In any case chances are that the charge to mass ratio of the actual mixture of ions is smaller that H^+. Hence the ion beam is probably slower than assumed in the computation, and in reality it should take longer for the pinching process to occur.

Residual gas in the diode gap may also supply ions. While the electron-ion ionisation cross sections are insufficient to account for appreciable ionisation it is possible that ultraviolet light generated by electron bombardment of the anode ionises the background gas. Again a code modification is needed to represent gradual introduction of plasma into the diode.

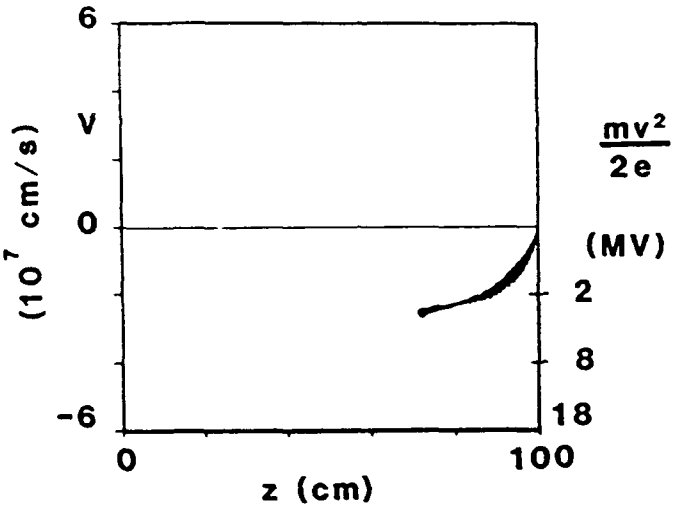

Figure 6. Ion phase space: p_z vs z at 37.5 ns.

2.3 CONCLUSIONS.

With some insight gleaned from the simulations presented here it is possible to suggest a few remedies to the anode destruction problem. First, there is no emission of light ions if there is no adhesion or absorption of these species on the anode surface. Then the electric field at the anode will not be able to pull any (light) ions off the surface, and there will be no charge neutralisation. While in the pulse power community a dirty vacuum and thus filthy surfaces seem to be a standard, a theoretician may rightly wonder what can be done practically with some gettering in judicious places, etc. Along the same lines is the suggestion to replace the residual gas with a gas that is hard to ionise, e.g. helium, and to change the surface of the anode to one that emits relatively little ultraviolet light on electron impact. Insufficient information prevents selection of a particular material here.

Another possiblility to avoid pinching could come from a modification in the diode geometry that might keep the electrons away from the axis. Attempts at such modifications have been tried in the simulations without success.

It is gratifying that qualitatively the pinch scenario is essentially the same as in low-impedance diodes. Without ions the electron space charge prevents pinching; introduction of ions cancels the space charge, and allows magnetic pinching to take over. In the present case, however, the pulse length is comparable to the time the ions need to cross the gap, and short compared to the time any anode blowoff would

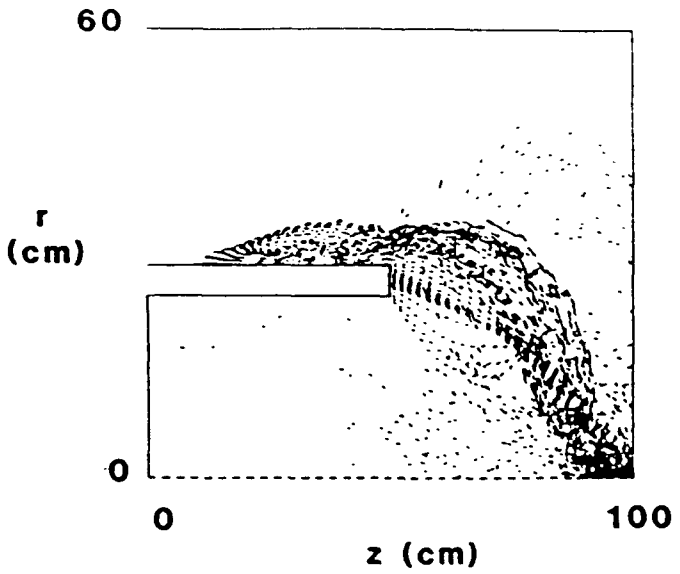

Figure 7. Electron trajectories after pinching, at 50 ns.

need to reach the cathode, at $4cm/\mu s$. Hence there is no appreciable ion current at the expense of the electrons, or a quasi-stationary pinch state. Hence it appears possible to avoid catastrophic pinching by one or more of the measures suggested above.

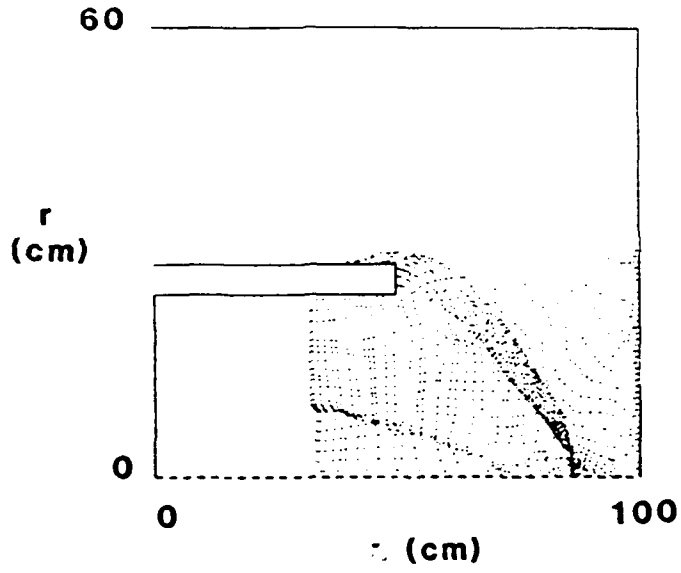

Figure 8. Ion trajectories after pinching, at 50 ns.

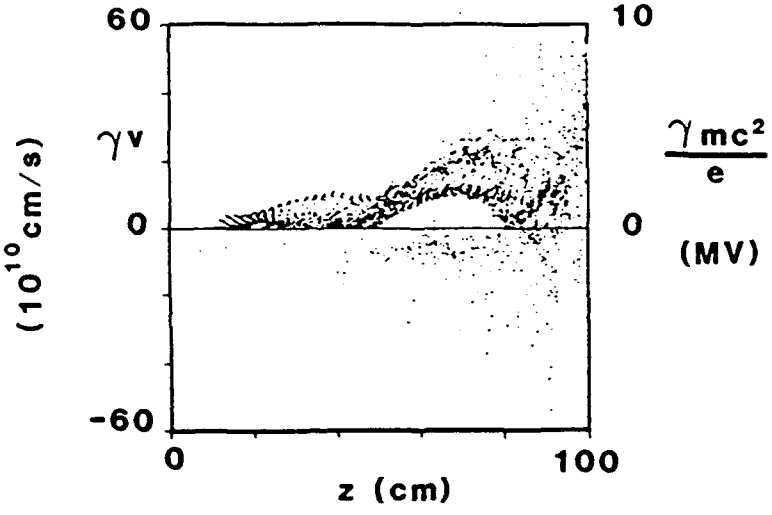

Figure 9. Electron phase space p_z vs. z.

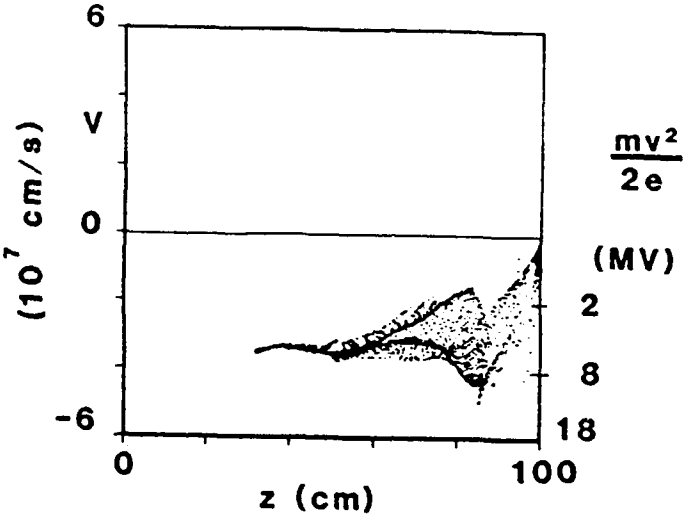

Figure 10. Ion phase space p_z vs. z.

2.4 CODE INPUT

```
comment * aurora diode simulation * /
title * paur * /
restart 3500 0 /
timeout 50 1 /
system 2 /
fields 1        3           3500        0.025e-9
                0.5         0.5         0.0
                3           1.0         0.2         0.1111 /
xlgrid 1        82          2           0.
                34          0.01850     0.5
                            46          0.01100     0.5
x2grid 1        68          2           0.
                36          0.00750     0.27
                30          0.00750     0.30 /
symmetry axial              1           2, 2        82, 2 /
conductor cathode           1           2,38        36,38 /
conductor cathode           1           36,38       36,33 /
conductor cathode           -1          36,33       2,33 /
conductor cathode           1           2,33        2, 2 /
conductor anode             -1          2,68        82,68 /
conductor anode             -1          82,68       82, 2 /
comment * slowly rising voltage * /
comment * mock-up aurora pulse * /
voltage         v(t)        v(r)        1.0         twod
                0.0         1.0         1           2,38        2,68        2 /
function        v(r)        5           -1          1.0 /
function        v(t)        0           11
                0.0         0.0
                10.0e-9     3.0e6
                20.0e-9     5.0e6
                30.0e-9     8.0e6
                40.0e-9     10.0e6
                50.0e-9     11.0e6
                60.0e-9     12.0e6
                70.0e-9     11.0e6
                80.0e-9     9.0e6
                90.0e-9     7.0e6
                100.0e-9    5.0e6
particles emission null electrons
                0           0           4           3
                1           2           1
```

```
                1.75e7          2.5e-7          1.25e7
                0               0               0               0
                1               8,38            36,38 /
particles emission null ions
                1               1               1               17
                1               2               1
                1e5             2.5e-5          2e5
                0               0               0               0
                -1              82,42           82,2 /
particles emission null electrons
                0               0               4               3
                1               2               1
                1.75e7          2.5e-5          1.25e7
                0               0               0               0
                1               36,38           36,33 /
particles emission null electrons
                0               0               4               3
                1               2               1
                1.75e7          2.5e-5          1.25e7
                0               0               0               0
                -1              8,33            36,33 /
comment * numerix data * /
courant         0               0 /
kinematics      1               0               0               0               4 /
com_ ient * diagnostics * /
trajectory      250             1               1.0
                0.0,1.0                         0.0,0.6 /
phasespace      250             24              1
                0.0,1.0                         0.0,0.6
                -5.5e9,5.5e9                    -5.5e9,5.5e9                    -5.5e9,5.5e9 /
phasespace      250             31              1
                0.0,1.0                         0.0,0.6
                -5.5e9,5.5e9                    -5.5e9,5.5e9                    -5.5e9,5.5e9 /
phasespace      250             24              2
                0.0,1.0                         0.0,0.6
                -5.5e7,5.5e7                    -5.5e7,5.5e7                    -5.5e7,5.5e7 /
phasespace      250             31              2
                0.0,1.0                         0.0,0.6
                -5.5e7,5.5e7                    -5.5e7,5.5e7                    -5.5e7,5.5e7 /
comment * voltage obtained by integrating e1 and e2 separately * /
contour         250             1 2 ,           2               82,68
                1 2             5               0               0 unity /
contour         250             2 2 ,           2               82,68
```

```
            2 2         5           0           0 radius /
comment * contour of b-theta, the current * /
contour     250         6 2 .       2           82.68
                        0 0         5           0           0 actr /
comment * contour of integral r rho dr and r j1 dr * /
contour     250         10 2 .      2           82.68
                        2 2         5           0           0 radius /
contour     250         7 2 .       2           82.68
                        2 2         5           0           0 radius /
function unity 1 1 1. /
function radius 5 1 1 1.0 /
observe     10          0           twod
            1           0           1           0           1
            2           2.38                    2,68 /
observe     10          0           twod
            1           0           1           0           1
            1           36,38                   82,38 /
observe     10          0           twod
            1           0           1           0           1
            6           68,61                   68,61 /
observe     10          0           twod
            1           0           1           0           1
            6           2,61                    2,61 /
range       250         1           2           2,38        2,68        0 /
range       250         1           1           68, 2       68,68       0 /
range       250         1           2           68, 2       68,68       0 /
range       250         1           6           68, 2       68,68       0 /
range       250         1           6           31,38       31,68       0 /
range       250         1           1           31,38       31,68       0 /
range       250         1           2           31.38       31.68       0 /
range       250         1           6           30.38       33.68       0 /
range       250         1           1           30.38       30.68       0 /
range       250         1           2           30.38       30.68       0 /
diagnose
                        spacing 0 1
                        courant 0 1
                        kmatrix 0 1
                        pbounds 0 1 /
statistics              250 /
balance                 250         2.2         82.68 /
flux                    250         1           36.38       36.68       0 /
flux                    250         1           81.2        81.10       0 /
flux                    250         1           81.10       81.20       0 /
```

```
flux                250     1       81.20   81.33   0 /
flux                250     1       81,33   81,40   0 /
flux                250     -1      81.2    81,40   0 /
display     1       2,82            2,68 /
comment * begin the simulation * /
start /
stop /
```

SECTION 3

DIODE CODE DEVELOPMENT

3.1 INTRODUCTION.

Recently the electromagnetic paricle simulation code MAGIC has become available to the DNA pulse power community. Over the past several months we have become familiar with the utilization of this code and have developed, implemented and tested modifications that allow us to begin modeling plasma radiation source (PRS) diodes. Our initial approach was to model the plasma load as an imposed axial current density. This required that MAGIC be extended to include in the simplest case a stationary axial current density profile $j_z(r)$ and more appropriately a time-varying profile $j_z(r,t)$.

The first modification to MAGIC was to include a stationary, uniform axial current density carried within an annular ring. For this configuration the imposed azimuthal magnetic field B_θ is zero interior to the ring, has a component that is directly proportional to r and a component that is inversely proportional to r exterior to the ring. Our approach was to modify the Lorentz force on the particles to include the analytic form for this imposed B_θ. Section 3.2 presents our implementation and tests of this modification. The three cases described in this section are: no imposed current; +200 kA current; and -200 kA current. As expected there is increased pinching in the +200 kA case and loss of magnetic insulation in the -200 kA case. The sudden appearance of a large magnetic field without the corresponding inductive electric field is unrealistic. Therefore, implementation of a time-varying current would be more appropriate.

The second modification to MAGIC was to include a time-varying axial current density profile. Our approach in this modification was to add the imposed spacially and temporally varying current density to that calculated from the particles. Consequently, proper inclusion of the induced electric field would be handled by the existing field solvers in MAGIC. Section 3.3 presents our implementation and test of this modification. For this case, we chose a current that rises to +200 kA during the first 5 ns and remains constant thereafter. As expected, the particle trajectories differ from the constant current case, but are qualitatively similar.

The third modification to MAGIC was to allow the deletion of diagnotics in a RESTART. Previously, it was only possible to add to the diagnostics. This created a situation where diagnostics that were no longer of value were required to continue through all subsequent RESTARTS. Our modification was designed to maintain the existing structure of MAGIC dataset handling. Section 3.4 presents our implementation and an example utilizing this modification.

3.2 MODIFICATION I.

A. Constant Axial Current

A stationary current I along the axis of a cylindrical diode as in Fig. 11 produces an additional magnetic field. The code can include the field as the initial value for the magnetic field to be read in, but it is simpler to modify only the Lorentz force on the particles. Moreover, the analytic form of the magnetic field allows accurate magnetic gradients for future use in drift orbit particle pushing.

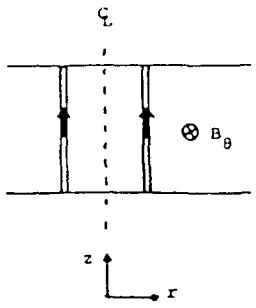

a. z-r view of axial current ring

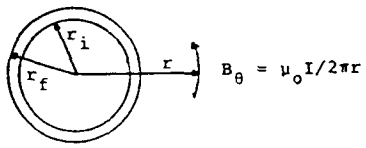

b. Cross section of current ring

Figure 11. Geometry for axial current.

The axial Z-pinch is modeled by a ring with constant current density

$$j_z(r) = \begin{cases} j_o, & \text{if } r_i < r < r_f; \\ 0, & \text{elsewhere.} \end{cases} \tag{1}$$

Ampere's law is

$$\frac{1}{r}\frac{\partial}{\partial r} r B_\theta = \mu_o j. \tag{2}$$

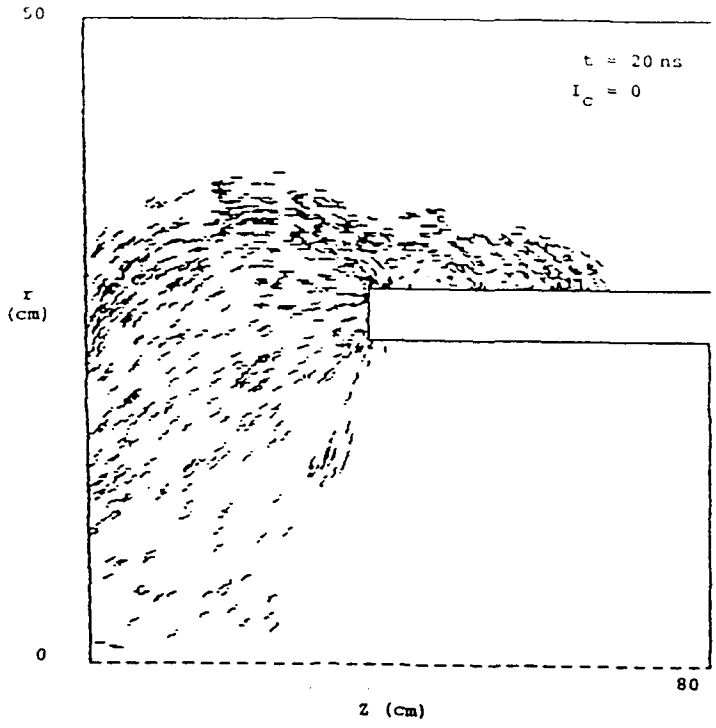

Figure 12. Initial state without axial current I_c.

with bondary condition $B_\theta = 0$ at the center $r = 0$. Then

$$B_\theta = 0 \qquad for \quad r < r_i, \tag{3a}$$

$$B_\theta = \frac{\mu_o I}{2\pi}(r - r_i^2/r)/(r_f^2 - r_i^2) \qquad for \quad r_i < r < r_f, \tag{3b}$$

and

$$B_\theta = \frac{\mu_o I}{2\pi r} \qquad for \quad r > r_f. \tag{3c}$$

The magnetic field outside the diode depends on the diode boundary, open return current structures or a closed cylindrical shell, but no interesting particles penetrate to these regions and this question will not be addressed here, except to point out that the typical θ-dependent return current configuration is felt inside the diode.

Equations (3) are implemented in the PIC code MAGIC by a subroutine CUREXT that is called before the particles are moved. Code modifications are shown in Section 3.2.B.

Figures 12, 13 and 14 show computational output solely as an example. An Aurora diode, 80 cm long, 50 cm outer radius, connected to a 120 cm long transmission line to a voltage source rising in 10 ns from 0 to 8 MeV, gives electron trajectories in Fig. 12 as expected. At time t = 20 ns, the particles suddenly see the additional magnetic field from Eq. (3) with current 200 and -200 kA; the result is expected, namely increased pinching in the 200 kA case, and loss of magnetic insulation in the -200 kA case. Of course, the sudden appearance of a large magnetic field without the corresponding inductive electric field is impossible; figures 12, 13 and 14 are intended to suggest that axial external currents can be included in the PIC code, and will produce interesting phenomena.

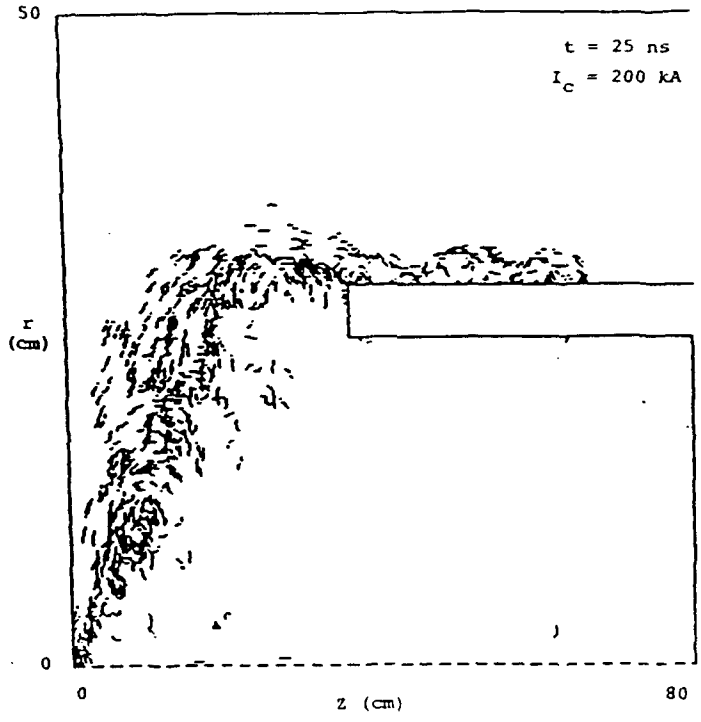

Figure 13. $I_c = 200kA$.

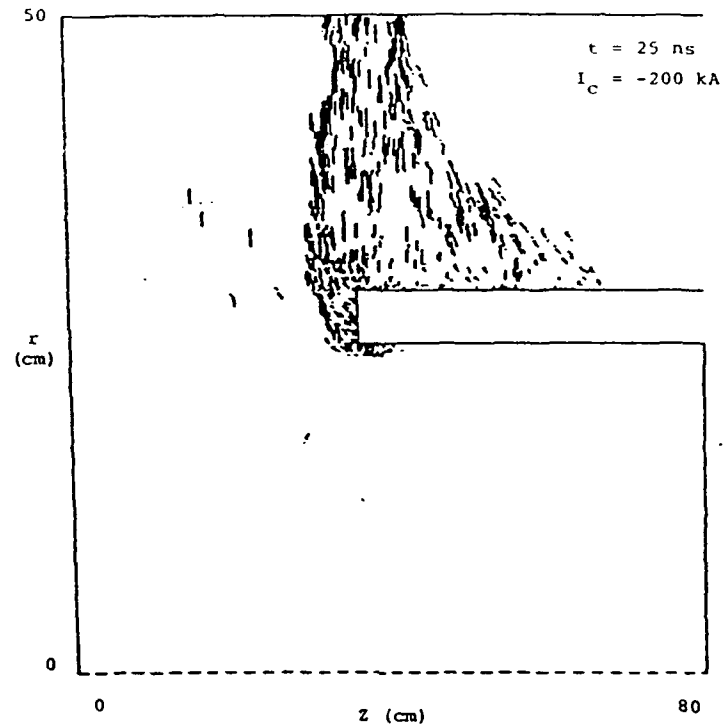

Figure 14. $I_c = -200kA$.

B. Listing of code modification

```
      subroutine curext
c ********** axial current gives magnetic field **********
c
c provides a magnetic field due to a constant axial current
c density in a ring with inner radius rinc and outer radius
c rfic with total current cure. the magnetic field is in the
c theta direction; hence, the routine works in the z,r,theta
c system (isym=2) only, where b-theta = b3.
c
c the constant external field bext should logically be
c implemented in the present routine rather than in the
c routine kinemat.
c
c ********** variable definition **************************
c
c cure   - axial current (amperes)
c rinc   - inner radius of current ring (meters)
c rfic   - final radius of current ring (meters)
c
*ca,common
cdir$ nolist
c
c only perform for cylindrical (z,r,theta) system
c when cure is non-zero.
c
c duplicate the next coding in subroutine contour for plotting.
      if (isys .ne. 2) goto 190
      if (cure .eq. 0.0) goto 190
c
      cmu0 = cure*xmu0/topi
      abri = abs(rinc)
      rfis = rfic**2 - rinc**2
c
      do 110 np=1,npgp
      rcur = x2pi(np)
      if (rcur .le. abri) goto 110
      if (rcur .ge. rfic) goto 120
      b3wf(np) = b3wf(np)+cmu0*(rcur-rinc**2/rcur)/rfis
      goto 110
120   b3wf(np) = b3wf(np)+cmu0/rcur
110   continue
```

```
190     continue
c
c add constant external b-field here (to be implemented)
c
        return
        end
```

3.3 MODIFICATION II.

A. Time – Varying Axial Current

In contrast to a stationary current accompanied by a stationary magnetic field, a time-varying current gives an inductive electric field according to

$$\frac{\partial \mathbf{E}}{\partial t} = c^2 \nabla \times \mathbf{B} - \frac{\mathbf{j}}{\epsilon_o}; \tag{4a}$$

the magnetic field develops from

$$\frac{\partial \mathbf{B}}{\partial t} = -\nabla \times \mathbf{E}, \tag{4b}$$

and for a current that becomes stationary after some time the final magnetic field should be stationary and balance the j-term in Eq. (4a).

The current density **j** in Eq. (4a) in the unmodified code comes from the available particles. The modification is to add, in subroutine JEXTERN, an axial current density

$$j_z(r,t) = j(r)I(t) \tag{5}$$

to the particle current density; $j(r)$ is the radial current profile, determined by a function statement, and $I(t)$ is the time variation. The radial profile is normalized such that

$$\int j(r) dv_r = 1. \tag{6}$$

In Eq. (6) dv_r is the surface element, $d(\pi r^2)$, in the radial direction (x_2 for isys = 2) that is available in the code (1/vli2). The function $I(t)$ can then be given in amperes.

The actual coding is attached. Not that in the code the variable j_l is proportional to the current density but includes various factors. In subroutine JEXTERN, j_l = current density x volume x timestep = charge displacement in a timestep. In subroutine JBOUNDS, j_l is turned into j_l = - current density x (dt/ϵ_o), in addition to enforcement of the boundary conditions.

Figures 15 and 16 give the output for a sample problem. In this case the current rises to 200 kA during the first 5 ns, and remains constant thereafter. The particle trajectories (Fig. 15) differ from the constant current case but are qualitatively similar, in particular the large vortex between anode and cathode tip. The magnetic field (B_θ) contours (Fig. 16) are as they should be, bunched about the axis, and straight except close to the particles. Contours 2 and 3 give the correct magnetic field (assumed stationary) of 0.44T and 0.7T respectively.

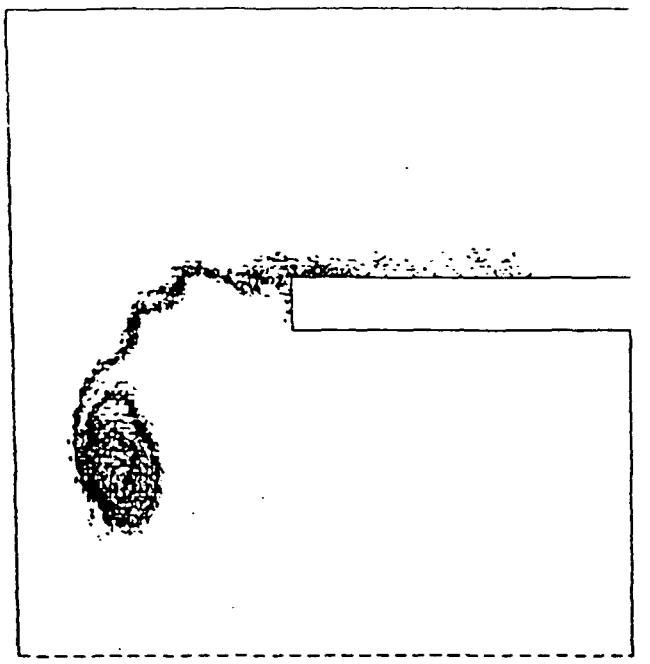

Figure 15. Electron trajectories. Magic simulation at time 1.50E-08 seconds for 4 time steps.

Potential inaccuracies in the simulation are suggested by the many "wiggles" in the contours, and by the convergence of the contours to the axis at the right edge. This last feature is due to the perfectly conductive boundary at that edge, which wants to put an image current on the other side that cancels the applied current. Other boundary conditions exist in the code that are more appropriate.

The test problem is sufficiently unphysical that we should not worry about the physical details, such as boundary conditions, wiggles, and such. We conclude that the additional axial current is included properly.

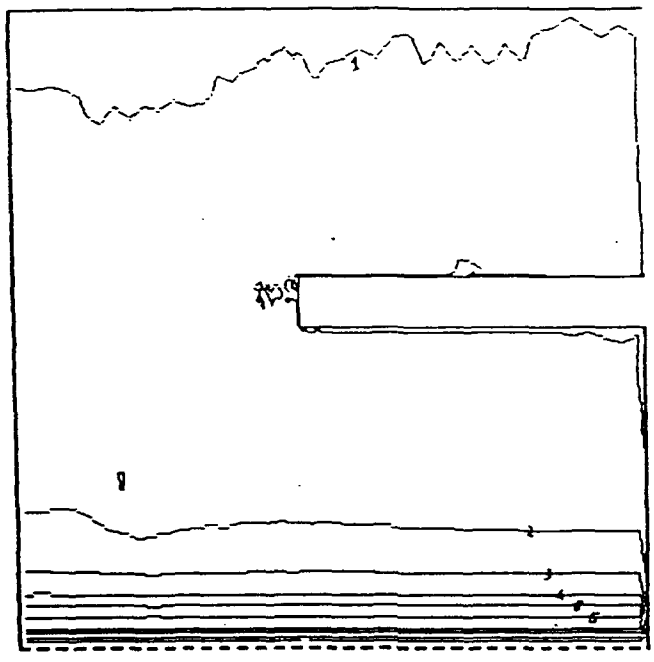

Figure 16. B_θ contours. Magic simulation at time 1.50E-08 seconds for contour intervals of 2.70E-01 (MKS).

B. Listing of code modification

```
c
      subroutine jextern
c
c ******* external current density j(r,t) along axis ******
c gives an external current density profile (dependent on r=x2)
c changing in time along the z-axis in a cylindrical
c
c      z,r,theta (isys = 2)
c
c system only, radial and time dependence in through
c      ajlx    ajlt
c the current density is normalized to this total
c current at each time step.
c
c ******* variable definitions ******************
c
c curf   - total current in current density profile/normalization
c jl     - current density * cell volume * dt
c curt   - applied axial current dependence on time (amperes)
c cdxr   - radial dependence of the current density
c
c
*ca.common
cdir$ nolist
c
c
c the first time around, initialize the current density
c array cdxr, and normalize to 1 ampere
      if (isys .ne. 2) goto 900
      if (nctx .eq. 0) goto 900
      if (curf .ne. 0.) goto 200
c
      do 120 i2=1,i2mx
      call functio(ajlx,x2hg(i2),cdxr(i2))
120   continue
c
c find total current represented by given profile
      do 130 i2=1,i2mx
      curf = curf+cdxr(i2)/v1i2(i2)
130   continue
      if (curf .ne. 0.) curf = 1./curf
```

```
c
c set external current density in radius and time
200     continue
        call functio(aj1t,trun,curt)
        temp = -curf*curt*dtim*ftaj/eps0
c
        l = 1
        do 210 i2=1,i2mx
        do 210 i1=1,i1mx
        j1(l) = j1(l)+temp*cdxr(i2)/(v1i1(i1)*v1i2(i2))
        l = l+1
210     continue
c
c j1 contains current density * cell volume * timestep
c j1 is turned into a source term for curl e in current
c boundary routine, next step.
c
900     continue
c
        return
        end
```

3.4 MODIFICATION III.

A. Modified Diagnostics in a RESTART

In the present version of MAGIC it is not possible to modify all input parameters and diagnostics in a RESTART. However, it is possible to add to the diagnostics, and the result is much more output than desired. To avoid this problem, we have added a DELETE feature that allows the code user to delete certain input functions and output diagnostics. MAGIC counts the number of these functions and diagnostics, in subroutine DATASET, and DELETE simply reduces the count by the desired number.

The dataset definition is

DELETE	ADEL	NDEL
ADEL -	alphanumeric label of dataset to be deleted.	
NDEL -	number of these deleted datasets.	

The coding, a block in subroutine DATASET, is attached. For example, in the original run you have specified 3 contour plots; on RESTART, you want to change the contour interval on the second plot, and the third plot is useless so you want to delete it. To the input data on RESTART you add

DELETE CONTOUR 2

and after this element you add

CONTOUR (modified parameters).

The diagnostics on RESTART will contain the first contour, and the contour plot specified in the RESTART; the third will have disappeared.

Elements that can be deleted by the present MAGIC modification are:

COMPLOT	LINPRINT
CONTOUR	LOGPRINT
DIAGNOSE	OBSERVER
DISPLAY	PHASESPACE
FLUX	RANGE
FUNCTION	

As an example, in Fig. 17 are the electron trajectories after a restart with a changed time dependence of the axial current, going from 200 kA to -200 kA in 5 ns between 20 and 25 ns. The result is intermediate between the 200 kA case (I.2b) and the -200 kA case (I.2c), as expected.

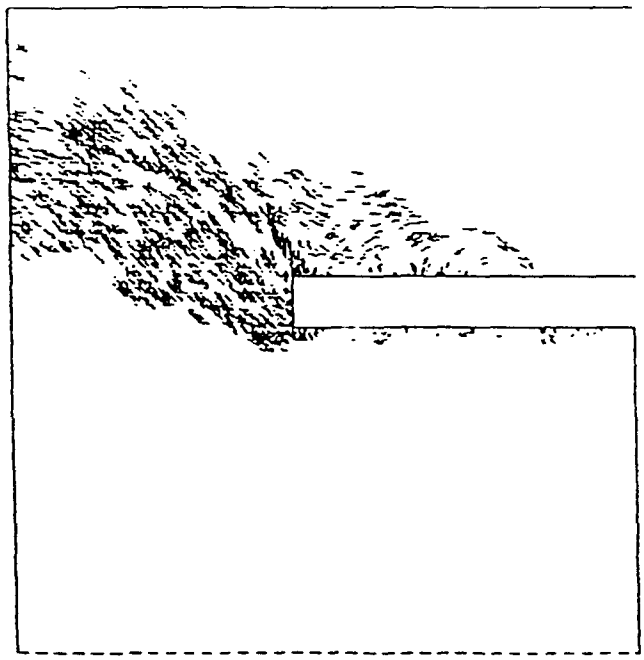

Figure 17. Electron trajectories. Magic simulation at time 2.50E-08 seconds for 4 time steps.

B. Listing of code modification

```
c
      subroutine dataset
                .
                .
                .
c
c ************ element delete ***********
c
c       (data sequence)
c
c delete adel ndel
c
c       (variable definitions)
c
c delete - element label for deleting datasets on a restart
c adel   - alphanumeric label specifying what to delete
c delchar character variable containing adel
c ndel   - number of 'adel's deleted
c
c as an example, if one diagnostic turns out to be useless
c for your run it can be deleted on restart; if the
c diagnostic is the middle of three in the initial
c specification, the last two must be deleted, and the last
c one must be resupplied. to modify a diagnostic you must
c delete it, and then resupply a new diagnostic in its place.
c
c
                .
                .
                .
      else if (valchar .eq. 'delete') then
      nv = 1
      write(delchar,997) valu(1+nv)
      ndel = valu(2+nv)
      ndel = max0(0,ndel)
      nv = nv+2
c
      if (delchar.eq.'complot') then
            ncpl = max0(0,ncpl-ndel)
            goto491
      else if (delchar .eq. 'contour') then
```

```
                nctr = max0(0,nctr-ndel)
                goto491
        else if (delchar .eq. 'diagnose') then
                ndos = max0(0,ndos-ndel)
                goto491
        else if (delchar .eq. 'display') then
                ndis = max0(0,ndis-ndel)
                goto491
        else if (delchar .eq. 'flux') then
                nflx = max0(0,nflx-ndel)
                goto491
        else if (delchar .eq. 'function') then
                nfun = max0(0,nfun-ndel)
                goto491
        else if (delchar .eq. 'linprint') then
                nlin = max0(0,nlin-ndel)
                goto491
        else if (delchar .eq. 'logprint') then
                nlog = max0(0,nlog-ndel)
                goto491
        else if (delchar .eq. 'observe') then
                nobs = max0(0,nobs-ndel)
                goto491
        else if (delchar .eq. 'phasespace') then
                npha = max0(0,npha-ndel)
                goto491
        else if (delchar .eq. 'range') then
                nrng = max0(0,nrng-ndel)
                goto491
c trying to delete invalid function
        else
c
                if (lsup(isup) .ne. 1) then
                write(6,120) ndel,delchar
                goto 200
                endif
                endif
        491     continue
c
c function deleted: write name
        if(lsup(isup).ne.1) then
        write(6,121) ndel,delchar
        endif
```

```
c
      call datasum(0,nv,nval,0,0,0)
c
```

SECTION 4

LEAKAGE CURRENTS OUTSIDE AN IMPLODING Z-PINCH

4.1 INTRODUCTION.

It is important to know where the current flows in a radiating z-pinch[1]. Experimentally, the emission of kilovolt x-rays is roughly proportional to the fourth power[2,3] of the current, whence a small shunt current could have a surprisingly large and deleterious effect on the pinch's radiation output. A quantitative estimate of the shunt current is the purpose of this paper. The current outside the z-pinch plasma is generally thought to be negligible. For relevant parameters (e.g. $I \sim 1\ MA$ and pinch radius $r \sim 1\ cm$) there is a large magnetic field in the vacuum outside the pinch ($B \sim 10\ T$), and this B_θ field should provide magnetic insulation. As shown below, however, magnetic insulation in a cylindrical z-pinch diode is not necessarily complete under all circumstances. Whether leakage currents affect the pinch's radiation output depends primarily on the amount of material relative to that in the pinch, that is, the initial conditions in a particular experiment.

In the initial phase of the electrical pulse the current through the pinch is small while the voltage is already appreciable. Under these circumstances there is a transient electron current analogous to the uninsulated front of a magnetic insulation wave. Thereafter the current through the inductive load becomes sufficiently large to cut off this transient. Computer simulation indicates that the magnetically captured electron sheath rolls up into relatively stable vortices, see Section 4.2.

After this initial phase but still in the early stage of the pulse the z-pinch material is rapidly ionized, a complicated process outside the scope of this work. The current compresses and implodes the bulk of the plasma, but almost by definition the current density is low outside the main plasma. The implosion of the main plasma can be computed with the resistive magneto-hydrodynamic equations, with proper includion of radiation production and transport. However, in the computations the exterior of the plasma sometimes[4] behaves in an unphysical way: the plasma temperature outside the pinch T can exceed 100 keV, the plasma conductivity increases excessively when using the standard Spitzer formula $\sigma \propto T^{3/2}$, and the high conductivity prevents the current from entering the z-pinch. The problem disappears when the conductivity is calculated properly, keeping into account the transition from a plasma dominated by collisions to a collisionless plasma (Section 4.3).

In this strongly magnetized, collisionless exterior plasma resistive hydrodynamics is invalid. Instead, the plasma electrons drift in the confining magnetic field $B_\theta(r)$ and the combined applied and space-charge electric field $\mathbf{E} = (E_z(z,r), E_r(z,r))$. The $E_z \times B_\theta$ drift inward generally dominates. The current density j_z

no longer satisfies Ohm's law, but instead is found by setting the power density $j_z E_z$ equal to the change in kinetic energy density, or equivalently, by taking the appropriate moments of the single particle distribution function The various current losses are small when there is little material outside the z-pinch. In order of magnitude, $I_{loss}/I_{total} \sim (N_{out} T_{out}/N_{pinch} T_{pinch})^{1/2}$, where $N_{pinch,out}$ is the number of particles in the bulk of the pinch (outside), and $T_{pinch,out}$ is the applicable temperature.

A reasonable mass per unit length for the z-pinch bulk is perhaps $100\mu g/cm$, while the particle density in the z-pinch periphery $n \sim 10^{13}/cm^3$ ($\sim 1\ mTorr$): over $100cm^2$ the mass per unit length in the outside the pinch is $\sim 0.01\mu g/cm$. Setting the typical temperatures about equal suggests a relative current loss of $\sim 1\%$, see section IV. Propagation of the electrical pulse through the exterior plasma isunder continuing study by one of us (RET).

In their inward motion the electrons keep the angular momentum p_θ constant, and therefore the electron velocity v_θ increases as $1/r$ and the parallel pressure $p_{||}$ as $1/r^2$. Also the magnetic moment $\mu = mv_\perp^2/2B \propto p_\perp/B$ is conserved. Therefore the perpendicular pressure $p_\perp$ increases with the magnetic field as $1/r$. The difference between the parallel and perpendicular pressure increases as the implosion of the collisionless plasma proceeds toward the center.

When the parallel and perpendicular pressure are unequal an exact self-similar oscillating pinch[5,6] is no longer possible. However, the oscillation remaines separable. The separable pinch has a low-density domain around the axis in response to the centrifugal potential that represents the non-zero angular momentum of the electrons (Section 4.5).

4.2 ESTABLISHMENT OF MAGNETIC INSULATION AROUND A Z-PINCH.

We have done computations on a generic z-pinch diode[7] that inspires the geometrical and pulse power parameters in the present work. The anode-cathode gap, 3 cm in this case, is bridged by an ideal conductor that mimics the z-pinch. The z-pinch radius, 0.6 cm, is representative of multiple wire loads[8] but substantially smaller than the initial radius of a gas puff.

In the computer simulations, performed with MAGIC[9], electrons are emitted from all cathode surfaces assuming space-charge limited flow, i.e. emission continues until the normal electric field vanishes. No ion emission is allowed.

The voltage at the diode entrance rises linearly on a 5 ns timescale to over 1 MV. The current satisfies $\dot{I}$=V/L and is quadratic in time, exceeding 100 kA at the end of the simulation, for a magnetic field at the z-pinch edge up to about 4 Tesla (40 kG).

The current in free electrons starts once the electric field in the diode feed exceeds 200 kV/cm. At this time, t=0.5 ns, the current through the z-pinch is insufficient for magnetic insulation, and the free electrons simply cross the diode gap. Later in time these electrons become trapped, and evolve until t=4.4 ns, the end of the pulse, the electrons are distributed in space as in in vortices. The magnetically insulated space charge sheath in the current feed appears to stream off the cathode into the diode already filled with previously emitted electrons. The sheath is clearly unstable, rolling up into vortex-like structures that persist as they move toward the center conductor. Qualitatively similar results are found in simulations with different parameters, e.g. a slower voltage risetime, or a smaller z-pinch inductance more representative of a gas puff.

There is an exact analogy between strongly magnetized non-neutral electron beams and inviscid fluid flow[10]. In two-dimensional Cartesian geometry with constant magnetic field B_z the charge density $\rho/\epsilon_0 B_z$ corresponds to the vorticity $\zeta_z = \nabla \times \mathbf{v}$. The electron fluid drift velocity $\mathbf{v_D}$ can be derived from the stream function ψ as $\mathbf{v_D} = \mathbf{e_z} \times \nabla\psi$, where $\nabla^2\psi = \zeta_z$.

The exact correspondence breaks down in cylindrical geometry because the magnetic field varies with radius r, $B_\theta = \mu_0 I/2\pi r$; now

$$\nabla \times \mathbf{v} = -\rho/\epsilon_0 B_\theta - E_r \frac{\partial(1/B_\theta)}{\partial r}. \qquad (7)$$

The last term is small compared to the first, except perhaps near the central conductor where the blob size is comparable to the geometrical scale. Hence in our diode the analogy with inviscid shear flow is largely valid.

The magnetically insulated space charge sheath coming off the cathode is an unstable vortex sheath. In fluid dynamics it is well-known how the instability develops, namely into coherent vortex regions reminiscent of the space charge blobs seen in our simulation. The blobs are stationary entities because the electrons remain on equipotential lines. The drift velocity $\mathbf{v_D} = \mathbf{E} \times \mathbf{B}$ is perpendicular to the potential gradient $\mathbf{E} = -\nabla\psi$, and $\mathbf{v_D} \cdot \nabla\psi = 0$. In a cylindrically symmetric blob the charge convected by the drifting electrons is then invariant, and the blob is a stationary entity. It is also known that isolated vortex regions are relatively stable.

Interaction between vortices is a strong mixing process[11]. The counterpart in our simulations should be a uniform spreading of the space charge blobs over the vacuum region of the diode. We have not studied vortex mixing because the pulse is over before mixing can be completed.

The leakage current in free electrons peaks at about 2 ns and decreases thereafter. The leakage current should be well approximated by the drift current parallel to the cathode in the thin space charge sheath that rolls off the cathode. In an insulating magnetic field B_θ the sheath electrons drift along the cathode into the

diode with the drift velocity $v_z \sim E_r \times B_\theta / B_\theta^2$. The electric field varies throughout the electron sheath from zero at the metal surface of the cathode to E_r at the top of the sheath, but the magnetic field is mainly from the central current, hence $B_\theta \sim I/2\pi r_i$. The current in the electron sheath I_e is then approximately $I_e = 2\pi r_i \sigma v_z$. The surface charge density σ of the cathode sheath is $\sigma = \epsilon_0 E_r$, where E_r is the normal electric field at the outside of the electron sheath. The sheath is thin compared to the pulselength width d, which is typically small compared to the inner radius r_i of the pulseline. Then the electric field can be approximated by $E_r = V/d$. Usually the inductive voltage dominates because the risetime τ is so fast, and $V = L\dot{I} \sim LI/\tau$ (L is the diode inductance, I the total diode current). With these approximations the relative importance of the electron current is

$$\frac{I_e}{I} \sim \left(\frac{E_r}{cB}\right)^2 \sim \left(\frac{r_i}{d}\right)^2 \left(\frac{Z_D}{Z_0/2\pi}\right)^2, \tag{8}$$

where $Z_0 = (\mu_0/\epsilon_0)^{\frac{1}{2}} = \mu_0 c = 377\ \Omega$, and Z_D is the total diode impedance.

The literature on magnetic insulation[12-14] contains estimates along the same lines as the above. In addition it is shown in detail that the single particle considerations used here correspond well to a treatment that includes the self-electric and -magnetic fields.

A typical z-pinch diode perhaps 3 cm wide, and the inductance $L \approx 6\ nH$. A typical pulse risetime may be $\tau \approx 12\ ns$, for a diode impedance of about 0.5 Ω. In contrast, the vacuum impedance $Z_0/2\pi = 60\Omega$, and the impedance ratio is 1/100. The electron current I_e is thus always a small fraction of the total current I, whence I_e can be ignored for imploding z-pinches.

For single exploding wires, in contrast, the vacuum current may become comparable to the conduction current. As an example, the inductance of a single $25\mu m$ radius wire load in a 3 cm wide diode is about 45 nH. For a fast 10 ns risetime pulse the factor $(Z_D/Z_0 \sim 0.1$, but a relatively small gap size partly compensates. When $r_i/d \approx 3$, for example, I_e/I of order 1/10. In this case there should be a sizeable leakage current in free electrons, potentially generating a measurable bremsstrahlung x-ray signal. Such a signal may have been observed[15] in in the Gamble II device at the Naval Research Laboratory, although no quantitative measurements are available. If corroborated by further work the bremsstrahlung x-ray signal may be an excellent indicator for the arrival time of the pulse.

4.3 TRANSITION TO COLLISIONLESS PLASMA.

The electron energy distribution function in the periphery of a radiating z-pinch is relatively easy to calculate by assuming that the electron-ion collisions isotropize the plasma electrons, but are unimportant in energy exchange between electrons.

Then the isotropic part of the electron distribution function f_0 satisfies a highly simplified form of the Fokker-Planck equation[16], viz.,

$$\frac{\partial f_0}{\partial t} - \frac{eE}{3mv^2}\frac{\partial}{\partial v}v^2 f_1 = C(f_0, f_0). \tag{9}$$

Here $C(f_0, f_0)$ is the Fokker-Planck collision temr for multiple scattering between electrons, f_1 is the anisotropic part of the electron distribution function $f = f_0 + f_1 + \cdots$ in the electric field direction $\mathbf{E}/\mathrm{E}$,

$$f_1 = \frac{eE}{m\nu_{ei}(1 + \omega_{ce}^2/\nu_{ei}^2)}\frac{\partial f_0}{\partial v}. \tag{10}$$

Here ν_{ei} is the electron-ion collision frequency, and the magnetic field B enters through the electron cyclotron frequency $\omega_{ce} = eB/mc$. The perturbation treatment is valid provided f_1 remains small compared to f_0.

Quantitatively, the transition to a collisionless plasma can be studied with a numerical solution of the isotropic Fokker-Planck equation, implemented according to Ref. 17. The distribution function changes in the transition from a collisional plasma, with low temperature, to a hotter plasma where collisions are no longer important. Eventually the distribution function approaches the asymptotic form[18] $f(\epsilon) \sim exp[-\epsilon^{5/2}/\epsilon_0^{5/2}(\tau)]$: for large ϵ the distribution function $f(\epsilon)$ decreases much faster than a Maxwellian. The normalized temperature $\epsilon_0(\tau)$ increases with time as $\tau^{2/5}$, and the electrical conductivity decreases with time:

$$\sigma(\tau) = \int_0^\infty d\epsilon f(\epsilon) \propto 1/\tau^{3/5}. \tag{11}$$

The temperature and conductivity versus time eventually reach an asymptotic state.

How long it takes the plasma in the z-pinch periphery to reach this asymptotic state depends largely on the initial density. To our knowledge there are no measurements on the periphery of an imploding z-pinch. The initial gas density[19] may be on the order of $n_{gas} \sim 10^{13} - 10^{14}/cm^3$, 100-1000 times the base pressure. If the plasma were a hypothetical fully ionized neon at 1 eV the collision time would be 1 ns, and the electron distribution reaches its asymptotic state in the pulse time ($\sim 10ns$). For fully ionized neon at 100 eV the collision time is 1 μs, whence the distribution function can not change during the pulse.

If a peripheral plasma were important for the character of the z-pinch implosion there should be some unexplainable difference between z-pinches that start from an injected gas on the one hand, and multiple wires on the other. Slight differences that have been observed can be accounted for by other factors than a current leakage in the pinch periphery. For example, each of the wires in a multiple-wire implosion blows up early in the pulse. Sometimes[20] the blow-off plasma is torn off and implodes on axis even before the bulk of the original wires has moved. The lack of

positive experimental evidence suggests but does not exclude that a plasma outside an apparently well-defined current channel has a negligible effect on the pinch.

The remainder of this paper assumes that the z-pinch periphery contains a collisionless plasma, with density and temperature to be determined. The magnitude of these parameters will determine whether the peripheral plasma is important in z-pinch implosions.

4.4 COLLISIONLESS CURRENT DENSITY.

In a collisional plasma the collisions are the dominant influence that balances the motion of the plasma electrons against the acceleration by the electric field. The resulting collisional electron drift, and thus the current density $\mathbf{j}$, is proportional to the electric field $\mathbf{E}$, namely $\mathbf{j} = \sigma\mathbf{E}$. The electrical power input into the plasma ends up in increased random velocities of the plasma particles, i.e., Ohmic heating.

Even in the absence of collisions the magnetized plasma in the z-pinch periphery can absorb energy from the electrical pulse. In this case the energy does not go into random motion of the plasma particles, but instead is put into organized motion. This motion was identified but not completely amalyzed under the present contract. However, much subsequent work has shown some interesting phenomena. Some of this is included here for completeness, and to give a perspective on how research changes direction in response to unanticipated results.

A strongly magnetized plasma in an electric field is not accelerated by the field, but drifts with a velocity $v = E/B$. For constant electric field the energy remains constant, but when the electric field increases in time the plasma accelerates. The kinetic energy density ρv^2 increases also (ρ is the plasma's mass density), and electrical power is absorbed. Likewise, electrons that $E \times B$ drift into a region of increased magnetic field spin up, increasing their perpendicular energy $w_\perp$ in an effort to keep the magnetic moment $\mu \sim w_\perp/B$ constant. The increase in $w_\perp$, or the increased magnetization, is another power sink.

The angular momentum about the axis, $P_\theta = mrv_\theta$, is conserved in a cylindrically symmetric geometry, and $v_{||}$ increases as $1/r$. A drift toward the axis increases the kinetic energy parallel to the magnetic field $w_{||} = mv_{||}^2/2$ as $1/r^2$.

Energy conservation is then expresed by the formula

$$j \cdot E \;=\; d(KE)/dt + \mathbf{v} \cdot \mathbf{F}, \tag{12}$$

where the pressure force is $\mathbf{F} = -\nabla.\mathbf{p}$, and $\mathbf{p}$ is the pressure tensor.

The macroscopic quantities that enter into the fluid equations are averages over the particle distribution function. Without collisions the distributions are not necessarily maxwellian, but the exact functional form is unimportant because only

the averages count. Instead of the distribution in terms of the velocity components in cylindrical geometry it is better to use the distribution function in terms of the dynamical invariants, the magnetic moment μ and the angular momentum P_ϑ. The distribution function is

$$f(r, \mathbf{v}, t) = \left[\frac{m^2 \, r}{2\pi \, B(r,t)} \right] \, n(r,t) \, F(\mu, P_\vartheta, r) \, . \tag{13}$$

The factor in $[\cdots]$ is the Jacobian of the transformation from the velocity vector $\mathbf{v}$ to the gyrophase angle ϕ, magnetic moment μ, and angular momentum about the axis P_θ. In the absence of collisions the magnetic moment is approximately conserved, but even with collisions P_θ is invariant. Then the distribution function F is constant in time. The particle density $n(r,t)$ is no longer part of F, which is normalised as

$$\left[\frac{m^2 \, r}{2\pi \, B(r,t)} \right] \int d\mu dP_\theta \; F(\mu, P_\theta, r) \; = \; 1, \tag{14}$$

for both electrons and ions. With the assumption of quasineutrality the mass density ρ is $\rho = (m_{electrons} + m_{ions})n(r,t)$.

The parallel pressure is

$$p_{||} \; = \; \rho L_{||}^2 = \int d\mu dP_\theta \; F P_\theta^2 / m^2, \tag{15}$$

and the perpendicular pressure becomes

$$p_\perp \; = \; \rho W_\perp = \int d\mu dP_\theta \; F\mu / m, \tag{16}$$

and the summation over species is understood.

The axial current density, calculated either by momentum balance or by averaging of nev_z, is then

$$j \; = \; \frac{\rho c^2}{B} \frac{D(E/B)}{Dt} + \frac{c}{B} \left[\frac{\rho L_{||}^2}{r^3} - \frac{1}{r} \frac{\partial (r \rho B W_\perp)}{\partial r} \right] . \tag{17}$$

The first term is related to the acceleration of the $E \times B$ drift motion, the second comes from angular momentum conservation, or $p_{||}$, and the third is the magnetization contribution, from $p_\perp$. In the acceleration term the ions dominate; the electrons are more important for the two pressure-derived terms without thermal equilibrium between electrons and ions. The effect of Eq. (17) on electromagnetic energy transport is presently under study by one of us (RET).

4.5 EXACT SEPARABLE IMPLOSION WITH $p_\perp \neq p_\parallel$.

For special initial conditions there exists[5,6] an exact solution to the fluid equations that describe strongly magnetized plasma in the periphery of a current-carrying z-pinch. These equations are standard,

$$\partial n/\partial t + \nabla \cdot (n\mathbf{v}) = 0, \tag{18}$$

$$\mathbf{v} = c\mathbf{E} \times \mathbf{B}/B^2, \tag{19}$$

$$\partial \mathbf{B}/\partial t = \nabla \times (\mathbf{v} \times \mathbf{B}), \tag{20}$$

and

$$\nabla \times \mathbf{B} = 4\pi \mathbf{j}/c. \tag{21}$$

However, in what follows the momentum equation includes an anisotropic pressure $\overleftrightarrow{p}$, $\rho d\mathbf{v}/dt = -\nabla \cdot \overleftrightarrow{p} + \mathbf{j} \times \mathbf{B}/c$.

An isotropic pressure implies that the collisions are sufficient to keep the velocity components randomized. This, then, implies a finite conductivity, in contrast to the assumption of infinite conductivity which demands a collisionless plasma. However, as the plasma gets closer to the axis in a cylindrical geometry the pressure $p_\parallel$ parallel to the magnetic field $B = B_\theta(r)$ increases as $1/r^2$, while the perpendicular pressure $p_\perp$ increases as $1/r$. In fact, in any curvilinear magnetic field an isotropic pressure is strictly speaking inconsistent with infinite conductivity.

The fluid equation of motion in the radial direction, for an anisotropic pressure, includes an centrifugal force $L_\parallel^2/r^3$ that reflects the conservation of angular momentum,

$$\rho \frac{DU}{Dt} = \frac{\rho L_\parallel^2}{r^3} - \frac{1}{r}\frac{\partial (r\rho B W_\perp)}{\partial r} - J_z B. \tag{22}$$

The centrifugal term is $L_\parallel = L_{\parallel,electrons} + L_{\parallel,ions}$, and for each species

$$\rho L_\parallel^2 = m \int d^3v f r^2 u_\theta^2, \tag{23a}$$

where u_θ is the particle velocity along the magnetic field. In terms of manifestly invariant quantities

$$\rho L_\parallel^2 = \rho \int d\mu dP_\theta \; F \frac{P_\theta^2}{m^2}. \tag{23b}$$

Likewise, the perpendicular pressure is connected to the kinetic energy perpendicular to the magnetic field,

$$\rho H_\perp = \rho B W_\perp = \int d^3v \; f m v_\perp^2/2, \tag{24a}$$

which is, in terms of the invariants,

$$\rho B W_\perp \;=\; \rho B \int d\mu dP_\vartheta \; F\mu/m. \tag{24b}$$

Equation (22) allows a selfsimilar oscillation of the pinch plasma[5] when the angular momentum $L_{||}$ vanishes, but even for non-zero $L_{||}$ a self-similar oscillation is possible. A comprehensive discussion of these solutions is deferred to a future paper[21], but here a simple example is shown.

Henceforth the dependent variables B, ρ, $L_{||}$, $W_\perp$ and their derivatives are functions of the single selfsimilar variable $\xi = r/a(t)$, where $a(t)$ is a typical scale length that contains the sole time dependence. Then Eq. (22) becomes

$$\frac{d^2\alpha}{dt^2} \;=\; \frac{\omega_{||}^2}{\alpha^3} + \frac{\omega_\perp^2}{\alpha^2} - \frac{\omega_A^2}{\alpha}, \tag{25}$$

where $\alpha(t)$ is the normalized scale length $\alpha(t) = a(t)/a_0$. Non-vanishing angular momentum is responsible for the term with $1/\alpha^3$, with $\omega||^2(\xi) = L_{||}(\xi)/\xi^4$.

In general the coefficients $\omega^2 = \omega^2(\xi)$ depend on the spatial variable ξ, and Eq. (25) does not separate. Separation is feasible only when $\omega_{||}^2$ is constant. Recall that $L_{||}^2$ is an average of $P_{||}^2$, where $P_\theta \sim v_\theta r$ is the particle angular momentum. Since $v_\theta \sim \omega_\theta r$ also $P_\theta \sim \omega_\theta r^2$: constant $\omega_{||}^2$ then implies a parallel temperature proportional to (radius)^2, and an initial angular momentum proportional to (radius)^4.

The perpendicular pressure term gives rise to

$$\omega_\perp^2 = -\frac{1}{\xi^2\rho}\frac{\partial[H_\perp(\xi)\xi\rho]}{\partial\xi}, \tag{26}$$

which should no longer be a function of ξ. In this term the spatial dependence of the density $\rho(\xi)$ can be played off against the perpendicular thermal energy $H_\perp(\xi) = B(\xi)W_\perp(\xi)$. Either ρ or $H_\perp$ can be chosen freely. It is easiest to separate the spatial dependence in $H_\perp$ by setting $H_\perp(\xi) = H_0/g(\xi)$. The mass density is then

$$\rho \;=\; \rho_0 \frac{g(\xi)}{\xi} exp\left[-\int_1^\xi dx x g(x)\right]. \tag{27}$$

The acceleration term contains the magnetic field through $\omega_A^2 = B^2/4\pi\rho a_0^2$, which is the transit frequency of an Alfvén wave though the scale size a_0. A constant ω_A^2 therefore implies a specific magnetic field given by

$$\frac{d(\xi B)^2}{d\xi} = [B_\infty^2 \xi^2 g(\xi)]\; exp\left[-\int_1^\xi dx x g(x)\right]. \tag{28}$$

where $B_\infty^2 = 4\pi a_0^2 \omega_1^2 \rho_0$ is the magnetic field at the characteristic distance a_0. Equation (28) is really an expression for the total current enclosed by the pinch within a distance ξ, because $\xi B = 2I(\xi)/ca_0$.

The function $g(\xi)$ is arbitrary provided[21] that the density ρ be positive and finite everywhere, and that the various ω^2's remain positive. The simplest function to satisfy these requirements is $g(\xi) = \xi^2$. Then the various integrations can be done in closed form. For example, the density becomes

$$\rho = \rho_0 \xi exp - (\xi^4 - 1)/4, \tag{29a}$$

where ρ_0 is given by the mass per unit length within ξ. Then the mass per unit length within ξ is given by

$$2\pi a_0^2 \int^{\xi} d\xi \; \xi\rho \;=\; \sqrt{2}\pi a_0^2 \rho_0 e^{1/4} \gamma(-1/4, \xi^4/4). \tag{29b}$$

where $\gamma(a, x)$ is the incomplete gamma-function. Likewise, the current carried by the corona out to ξ becomes

$$I^2(\xi) - I^2(0) = \frac{c^2 a_0^2 B_\infty^2 e^{1/4}\sqrt{2}}{4} \gamma(1/4, \xi^4/4), \tag{30}$$

where $I(0)$ represents the current carried by a collisional pinch located on axis. This is reminiscent of the Bennett pinch relation, $I^2 \propto NT$, for good reason: The corona contributes its pressure to the current carrying capacity of the pinch.

4.6 SUMMARY AND CONCLUSIONS.

Current can be carried in the periphery of a z-pinch by various mechanisms. Initially the z-pinch carries no current, and the inductive voltage at the edge of the cathode away from the pinch material can drive a currrent in free electrons. The free electrons can be the bulk of the current at the very start, but this current is cut off rapidly once the current starts flowing through the z-pinch.

The tenuous plasma outside the z-pinch can also carry current. As a remnant of background gas or perhaps the edge of the injected gas column in a puff-gas z-pinch, this plasma is not well-specified either experimentally or theoretically. How much current is shunted through this plasma depends linearly on the plasma density, and also on parameters such as the temperature and the magnetic field in the periphery, i.e. the current in the main z-pinch.

The plama temperature in the periphery is computed from a simplified Fokker-Planck analysis, assuming that the electron velocity remains isotropic through collisions with the ions. Plasma heating proceeds until the electron collision time is

comparable to the pulse time, resulting in a temperature limit of something like 50 eV (weakly dependent on plasma density).

The pressure of the collisionless plasma in the periphery becomes anisotropic as the plasma contracts toward the axis, due to the separate conservation of the electron's magnetic moment, and the electron's angular momentum about the axis. Under these conditions the plasma can still oscillate in a self-similar manner, and for constant z-pinch current and balanced oscillation frequencies ($\omega_{\|}, \omega_{\perp}, \omega_{A}$) the periphery can be in an exact equilibrium.

As the current increases in the power pulse part of its energy is siphoned off by the periphery. How much depends on the plasma parameters, which are unknown. For a tenuous periphery, $n \leq 10^{13}/cm^3$, with the corresponding temperature, $T \sim 5.0eV$, little power is diverted from the z-pinch. For densities appropriate to edge gas, $n \sim 10^{15}/cm^3$, or higher temperatures $T \sim 50eV$,the power loss is substantial.

SECTION 5

LOW-INDUCTANCE PLASMA RADIATION SOURCE LOADS

Compact high-power electrical systems based on inductive energy storage for driving plasma radiation source loads depend on fast opening switches that must break many megamperes. This is no simple task even in the best of circumstances, but it is especially difficult when opening the switch generates a high voltage. An ideal opening switch would be able to decrease the current I to zero in a time τ, irrespective of the voltage this process generates. When the current is commuted into an inductive load L there appears a voltage spike with maximum $V_m \approx LI/\tau$ (in addition to any other voltage, e.g. a resistive voltage V = RI). In other words, when the current is not immediately diverted into a load the current will continue to flow in the switch. Depending on the physical characteristics of the switch the consequent energy deposition will modify the switch operation, usually for the worse. For example, the switch may restrike, or not open at all.

The punishment the opening switch is getting can be reduced by minimizing the inductance of the load circuit. Part of the minimisation involves simply geometry. A physical separation between the switch and the load implies an inductance $L \approx \mu_0 \ell \times G$, where ℓ is a typical length scale such as the switch-load distance, and G is a geometrical factor. Clearly, it is advantageous to make the switch-load distance as small as possible. One way to do this is by putting additional switches in the system that divide the inductance among themselves. Here we describe some ideas that may be useful in this general context.

A low-inductance wire load can be made by stretching wires between the outer edge of anode and cathode, followed by rotating one of the electrodes over an angle ϕ. No twist, or $\phi = 0$, gives a standard wire load, and $\phi \leq \pi$ creates the so-called X-pinch recently investigated by Soviet workers. Any angle in between 0 and π leads to wires with a hyperbolic envelope. Hence there is a continuous transition between the standard configuration and the X-pinch. The envelope can be expressed in terms of the twist angle ϕ, but the simplest way of doing this is in terms of the waist radius r_0 and the asymptotes with angle $tg\ \theta = z_0/2R_0$, where z_0 is the diode gap length and R_0 the electrode radius.

It is clear that the twisted wires have less inductance than wires strung straight between the electrodes at the radius r_0 of the hyperboloid's waist, but a larger inductance than wires at the electrode edges R_0. Optimum radiation production may require that the mass per unit length $\mu = m/\ell$ and the radius r are related by $\mu r^2 = C$, where C is a (machine-dependent) constant. In this case the inductance of the twisted wires is undoubtedly more favorable than the straight wires.

Twisting the wires only in the positive direction will generate a magnetic field B_z along the machine axis: this can be cancelled by twisting the same number of wires in the negative direction.

As usual in pulse power it seems much simpler to try out the geometry than to simulate it numerically, especially if the angle-dependent features are to be kept. Assuming that the wires behave as their hyperboloidal envelopes makes life sufficiently simple to allow simulation on a 2-D hydromagnetics code.

Since the load geometry is a continuous function of ϕ it may be possible that the radiation is maximized at a value intermediate between 0 and π, e.g. at ϕ_0. Then the load concept has merit.

As with straight wire loads the radiation yield may be further increased by letting the mass per unit length change with axial position, i.e $\mu = \mu(z)$, with larger mass in the pinch center. However, the twisted wires load may be particularly suited for use in generators based on inductive energy storage, where the load inductance may make the difference between a failing or a succesful switch.

Another way to decrease the switch-load distance is by putting an intermediate switch in the space between the two. This can be done with wire loads. The standard PRS load is halfway down toward the center, but there is a second wire load on the outside of the electrodes where the switching takes place, at R_0. These wires should have the appropriate mass per unit length μ for them to reach the radial position of the PRS load wires at the desired switching time. Presumably, the outer "switch" wires divert the current from the load wires because of their smaller inductance. In the limit of infinitely many wires

$$\frac{L_{switch}}{L_{PRS}} = \frac{\ln(R_{switch}/R_0)}{\ln(R_{PRS}/R_0)}, \tag{31}$$

which is approximately $\Delta R/R_0 \ll 1$: for a finite number of wires the current is not as well diverted. In this more realistic case there is leakage of the magnetic field through the gaps between the switch wires, which adds to the inductance.

The material from the switch wires will not disappear but instead it may collide with the PRS wire load, or it may gather and cook on axis. To avoid any interference in radiation production by the switch material its Z should be small compared to the Z of the PRS load, e.g. $Z_{switch} \leq 6$: plastic or graphite should work.

For a change it seems easier to evaluate a moderately realistic simple 0-D model of such a switch enhancement than to do the experiment, but we haven't done it as yet. First we want to see what other people think of it.

The (solid or liquid) foil switch may become an interesting and useful topic for numerical modeling. In this switch a foil is blown across a small cathode-anode gap by $j \times B$ forces. In the models we are familiar with the bulk of the switch foil is presumed to remain solid, or at most it may become liquid, but there are little or no plasma effects. However, at the edge of the foil where it touches the inner (cathode) part of the pulseline it is hard to see how the foil can avoid becoming a plasma: especially when the foil starts to shoot over the edge in its opening act there are

mega-amperes flowing in an ever-thinning sheath of material, which is bound to become a highly conducting plasma that streaks across and into the cathode-anode gap, exactly what we are trying to avoid.

It seems crucial to switch performance how much plasma gets into the gap: if there is little the plasma should collapse on axis similar to our switch wires, but if there is too much an arc can be struck between the electrodes, and the switch never opens, i.e. never transfers the current to the load. We propose to study this part of the process more in depth, partly by using existing hydrodynamic codes with addition of the appropriate conductivity expressions. Another part of our efforts will be to use literature data for help in identifying the processes that dominate the arc plasma.

Past experience with arcs suggests that a comprehensive modeling of all the events in the "opening" of the foil switch will be exceedingly difficult, but it is still necessary to attempt exactly this.

SECTION 6

ELECTRON ENERGY DISTRIBUTION IN A Z-PINCH

6.1 INTRODUCTION.

State of the art computations on the radiation production of imploding z-pinches follow the standard hydromagnetic laws for conservation of mass and momentum, augmented by a complete accounting of the energy density as this changes due to compression, Joule heating, and radiation cooling. The plasma parameters are typically such that particle collision times are much shorter than macroscopic timescales, and on this basis the electron distribution function f(v) is assumed to be in equilibrium, i.e. $f(v)dv = 4\pi f(v)v^2dv$ is isotropic in direction and Maxwell-Boltzmann in energy. Electric fields or spatial gradients usually produce small deviations from Maxwellian, and the corresponding coefficients can be taken from the literature[22,23]. Also the atomic excitation rate are computed by integrating the excitation cross section with a Maxwellian electron distribution.

In the plasma periphery where the plasma density is thought to be low ($n_e \sim 10^{12}$-$10^{15}/cm^3$) and the electron temperature to be high ($T_e \gg 1$ keV ?) the collision time is large compared to the pinch time (100 μs vs. 100 ns). Clearly the electron distribution is not necessarily in equilibrium: in fact, f(v) behaves as $exp(-v^5/5v_{th}^5)$, and the plasma temperature v_{th}^2 increases in time as $t^{2/5}$. The electrical conductivity, defined by the temperature rise divided by the electric field energy E^2, then decreases with temperature as $T^{-3/2}$. This result solves a difficulty that occurs occasionally in the pinch periphery using the radiation-MHD equations.

In the edge of the plasma the density appears sufficient to suspect a Maxwell-Boltzmann equilibrium distribution, but inelastic collisions can give significant deviations from a Maxwellian. Inelastic collisions are typically less frequent than electron-electron collisions, $\nu_* \ll \nu_{ee}$. However, transitions between the first excited state and the heliumlike ground state in moderate atomic number elements (from neon to iron and beyond) produce the most interesting radiation. Helium-like ions can typically not be excited by the thermal electrons in the bulk of the distribution, but only by the electrons in the distribution's tail. Elastic collisions are relatively infrequent there and thus ionization has a surprisingly large and depressing effect on the distribution function's tail. Consequently, the actual excitation rate may be lower than calculated from a Maxwellian[24], but the amount of change depends on how the distribution functions are compared.

When the electron distribution function is allowed to change its temperature in response to the inelastic collisions the inelastic reaction rate changes with an appreciable factor that reflects the reduction in plasma temperature. However, with an external electric field to keep the temperature constant the reaction rate is almost

the same as without inelastic collisions. In both cases the distribution function's tail beyond the inelastic threshold is significantly depressed (the computations up to now use a single inelastic process).

Smaller numbers of electrons at energies higher than the main inelastic threshold should be observable by reduced radiation from more energetic excited states compared to the lower-lying states, and there may be inconsistencies between the plasma temperature determined from the different states on the basis of radiative rates computed from a maxwellian.

It should be emphasized here that the pinch axis is explicitly excluded from the considerations for the moment. Along the axis the magnetic field does not prevent electrons from running away in any strong electric field that may exist. Electron runaway will be studied with a Monte Carlo computer code.

6.2 FORMALISM.

The plasma of interest is spatially homogeneous and highly ionized, with an average ionization state Z=10 or higher. Electron-ion collisions are perhaps 10× more frequent than electron-electron collisions. Energy exchange between electrons produces the equilibrium Maxwellian shape of the electron distribution function after roughly 5 self-collision times[25]. In contrast, isotropy in the electron velocity vector is governed by elastic electron-ion collisions, and the distribution function should be almost isotropic while it relaxes toward equilibrium. Electron fluxes come from small deviations in isotropy: because of the fast electron-ion rate any anisotropy is assumed to be in equilibrium with its driver. Hence the fastest timescale is the electron-ion collision time $\tau_{ei} = \nu_{ei}^{-1}$, while the timescale for changes in plasma temperature may be on the order of the electron-electron collision time τ_{ee}. Unfortunately, the collision times are not very different, $\tau_{ei} \sim \tau_{ee}/Z$, and the region of validity of the approach taken here may be more limited than desirable.

The purpose is to define a reasonably complete but still analytically tractable model for the the electron energy distribution function in the presence of an electric field **E**, magnetic field **B**, and inelastic collisions. Simplifications include the neglect of any spatial gradients, the effect of magnetic fields on the collision integrals, energy exchange in elastic collisions between electrons and ions, the absence of plasma instabilities, etc. The plasma ionization rate and electrical conductivity can then be estimated, and modifications herein may motivate further numerical work. Table 1 contains the some relevant parameters for the plasmas of interest.

The equation for the anisotropic part of the distribution function $f_1(\mathbf{v})$ is[24,26,27]

$$f_1 = \frac{eE}{m_e \nu_{ei}} \frac{\partial f_0}{\partial v}, \tag{32}$$

where ν_{ei} is the electron-ion collision frequency,

$$\nu_{ei} = \frac{nZY}{v^3}. \tag{33}$$

The known symbols have their usual meaning, and Y measures the effective ionic size in multiple scattering with the Coulomb interaction, $Y=4\pi(e^2/4\pi\epsilon_0 m_e)^2 \ell n\Lambda$. with $\Lambda \sim 9n_D$ and n_D the number of electrons in the Debye sphere. Typically, $\ell n\Lambda \sim 10$. In terms of fundamental quantities $Y= c^4\ (8\pi r_e^2/3)\ \ell n\Lambda/6$, with r_e is the classical radius of an electron and the term in parentheses is the Thomson cross section. Electron-electron collisions can be included properly at tremendous expense in complexity and approximately by replacing Z by Z+1. Neither correction is necessary since electron-ion collisions dominate. The even less frequent inelastic collisions are also ignored.

The magnetic field **B**, always taken perpendicular to the electric field **E**, can be included easily by introducing an effective electric field $E_{eff} = E/(1 + \omega_{ce}^2/\nu_{ei}^2)$. with $\omega_{ce} = eB/m$. The anisotropic part of the electron distribution function is, in these approximations, determined explicitly from the isotropic distribution function f_0.

Relaxation toward equilibrium of f_0 follows the equation (e.g. Ref. 27, eq. 7.71b, or Ref. 24, 5.16)

$$\frac{\partial f_0}{\partial t} - \frac{eE}{3m_e v^2}\frac{\partial}{\partial v}(v^2 f_1) = S_0 + S_i, \tag{34}$$

where the electron-electron energy exchange is contained in S_0, and the inelastic electron-ion collisions are represented by S_i. S_0 is given by

$$S_0 = \frac{4\pi Y n}{v^2}\frac{\partial}{\partial v}[(\int_0^v f_0\ v'^2\ dv')\ f_0 + (\frac{1}{3v}\int_0^v v^2\ f_0\ v^2 dv + \frac{v^2}{3}\int_v^\infty \frac{f_0}{v}\ v^2\ dv)\frac{\partial f_0}{\partial v}]. \tag{35a}$$

Only inelastic collisions with large energy loss are considered, and therefore S_i is simply

$$S_i = -\nu_i\ f_0 + \textit{replacement term}, \tag{35b}$$

where the electron replacement term is such that the number of electrons is conserved. The ionization frequency $\nu_i = n^* \sigma_i v$, with n^* the density of the ions that can be excited, and σ_i the velocity-dependent excitation cross section.

Normalization results in the equation

$$\frac{\partial h}{\partial \tau} = \frac{1}{\xi^2}\frac{\partial}{\partial \xi}[\ Ch + (\ D + \frac{E^2}{E_0^2}\frac{\xi^5}{1 + \Omega^2\xi^6}\ )\frac{\partial h}{\partial \xi}] - s(\xi)h + \textit{replacement term}. \tag{36}$$

Here[25] $\xi = v/v_0$ and $v_0^2 = 3kT/m$. The distribution function $h(\xi,\tau) = f_0(v,t)v_0^3$, and time is scaled as $\tau = t/t_0$, where $t_0 = v_0^3 Z/nY = Z/\tau_{ee}$, basically the electron-electron collision time at the thermal speed v_0. The electric field E is normalized by E_0, which is the field that in a collision time t_0 produces a velocity change on the order of v_0, $eE_0t_0/m = v_0\sqrt{3Z}$. The normalized cyclotron frequency $\Omega = \omega_{ce}t_0/Z$ and typically $\Omega \gg 1$.

Relaxation due to electron-electron collisions[25] is described by the $C(\xi)$ and $D(\xi)$ terms only, with

$$C(\xi) = \int_0^\xi d\eta \eta^2 h, \tag{37}$$

$$D = \frac{1}{3\xi}\int_0^\xi d\eta\ \eta^4 h + \frac{\xi^2}{3}\int_\xi^\infty d\eta\ \eta h. \tag{38}$$

Numerical solution indicates[25] that an arbitrary initial distribution function becomes Maxwellian in approximately 5 Spitzer collision times.

The replacement term will not be used in this form of the equation, but will enter to conserve electron number when seeking a stationary distribution function.

An alternate form of the same equation is obtained by using the (normalized) energy $\epsilon = \xi^2$,

$$\sqrt{\epsilon}\frac{\partial h}{\partial \tau} = \frac{\partial}{\partial \epsilon}[\gamma(\epsilon)f + \beta(\epsilon)\frac{\partial f}{\partial \epsilon}] - \alpha(\epsilon)f + \alpha_\Delta f_\Delta. \tag{39}$$

Here the coefficients are

$$\gamma(\epsilon) = D(\xi) = \int^\epsilon \epsilon^{1/2} f\, d\epsilon, \tag{40}$$

$$\beta = \frac{2}{3}[\int_0^\epsilon \epsilon^{3/2} f d\epsilon + \epsilon^{3/2}\int_\epsilon^\infty f\, d\epsilon + \frac{E^2}{E_0^2}\frac{\epsilon^3}{1 + \Omega^2\epsilon^3}. \tag{41}$$

The ionization loss coefficient α is

$$\alpha = \frac{n^*}{n}\frac{T}{Z^2\epsilon_R}\frac{4\Omega_{ij}(\epsilon)}{\ell n\Lambda}, \tag{42}$$

where Ω_{ij} is the collision strength for the atomic levels of interest, and ϵ_R is the Rydberg energy, 13.6 eV. The collison strength is connected to the inelastic cross section by

$$\sigma^* = \pi a_0^2 \frac{\Omega_{ij}}{Z^2}\frac{\epsilon_R}{\epsilon}, \tag{43}$$

and any multiplicity of levels is suppressed. The excited state ionic density is n^*. In this form of the equation the replacement coefficient becomes simply $\alpha_\Delta(\epsilon) = \alpha(\epsilon + \epsilon_i)$, where ϵ_i is the excitation energy.

Eventually the single inelastic cross section will be replaced by a summation over all the processes going on, including the super-elastic collisions that put energetic electrons back into the plasma, and collisions that absorb little energy per interaction but that collide fairly often. For the present purpose these processes are distracting, and they will be dealt with later.

The following treats two special cases of Eq. (39), the first relating to the plasma periphery where the collision energy exchange terms C and D are appropriate (though negligible), and the distribution function changes in time. The second case treats the plasma in the pinch edge away from the axis, where the distribution function reflects a stationary balance between collisional energy redistribution and ionization.

6.3 PINCH PERIPHERY.

In the pinch periphery the collision time is much larger than the pinch time, and the distribution function is no longer in equilibrium. Instead, the distribution function changes on a timescale much faster than τ_{ee}. Inelastic processes can be ignored, but the magnetic field is sufficiently strong to avoid electron runaway, i.e. $\Omega \gg 1$. The opposite case, electron runaway, is an old but still active research topic that is not at issue here.

A numerical solution with parameters $\Omega^2=1$ and $E^2/E_0^2=1$ was done to see the effect of heating. Initially the distribution was cold enough for the collision time to be comparable or smaller than the timescale for heating, and the distribution remained close to maxwellian. Eventually the plasma heated up enough for the collision time to become large compared to the heating time. The temperature increases at an ever decreasing rate.

Without collisions the heating can be calculated analytically. In this case the relevant equation for f_0 becomes, setting C and D to zero,

$$\frac{\partial h}{\partial \tau} = \frac{(E/\Omega E_0)^2}{\xi^2}\frac{\partial}{\partial \xi}\left[\frac{\xi^5}{\Omega^{-2} + \xi^6}\frac{\partial h}{\partial v}\right]. \tag{44}$$

A self-similar solution is possible for $\Omega\xi^3 \gg 1$, i.e. excluding the low-velocity regime where the abridged equation is not valid anyway. Ignoring Ω^{-2} in the denominator the self-similar solution is[28,29]

$$h \propto \xi_0^{-3}\exp(-\xi^5/5\xi_0^5). \tag{45}$$

where $\xi_0(t)$ increases with time according to

$$\xi_0^5 = \xi_0^5(0) + 5\int_0^t \left(\frac{E}{E_0\Omega}\right)^2 dt. \tag{46}$$

When the $\exp(-\xi^5)$-dependence is extended to small ξ, conservation of electrons gives the factor ξ_0^{-3}. The energy per particle, $\int \xi^4 h \, d\xi = \overline{\xi^2} = T$, the temperature, is then increasing in time more slowly than linear, $\overline{\xi^2} \propto t^{2/5}$. The (normalized) power input per particle decreases with time according to

$$\frac{\partial \overline{\xi^2}}{\partial t} = \frac{2}{5} t^{-3/5} \propto T^{-3/2}, \tag{47}$$

the opposite temperature dependence than found for the Spitzer conductivity. The conductivity as defined here is σ=(power input/E^2), which is $\partial\overline{\xi^2}/\partial t$, since the heat capacity is constant.

That the temperature dependence of the conductivity differs from the usual result should not surprise: the dominant effects differ. The Spitzer conductivity is found from a balance between the acceleration by the electric field and the collision time, assuming the temperature remains constant, while in contrast here the acceleration in a weakly collisional but highly magnetized plasma is balanced with the temporal development of the (non-equilibrium) distribution function.

The electrical conductivity in the plasma periphery used in the hydrodynamics computations should be replaced by the formulas obtained here as the changes in density and temperature in the periphery have brought the plasma in the weakly collisional regime. A reasonable transition point is when the collison time is 1-10 $\times$ the macroscopic timescale in the local plasma, e.g $\partial t/\partial \ell n T$ for the temperature increase. When the transition temperature T_c is reached in the MHD codes the available conductivity can easily be modified by simply replacing the temperature dependence from $(T/T_c)^{3/2}$ to $(T/T_c)^{-3/2}$, while keeping the constant at the transition temperature unchanged. Alternatively, the expression derived here can be used once it is smaller than the Braginskii conductivity. However, note that $(E/E_0\Omega)^2 = (v_0/v_D)^2 \times Z/12\pi \ll 1$, with v_D =E/B the drift velocity.

In the corona of laser-generated plasma measurements of the electron distribution function[30] show a flat-topped distribution in the energy regime accessible by the diagnostics, in agreement with the theory[26].

6.4 INELASTIC COLLISIONS.

This section estimates the decrease in ionization rate from the reduction in the distribution function's tail, with parameters relevant to the pinch periphery. From Table 1 it is apparent that a stationary distribution should exist on a nano-second timescale. The stationary distribution thus satisfies the equation

$$\frac{\partial}{\partial \epsilon}[\gamma(\epsilon) f + \beta(\epsilon)\frac{\partial f}{\partial \epsilon}] - \alpha(\epsilon) f + \alpha_\Delta f_\Delta = 0. \tag{48}$$

Here the coefficients $\gamma(\epsilon) = D(\xi) = \int^{\epsilon} \epsilon^{1/2} f \, d\epsilon$.

$$\beta = \frac{2}{3}\left[\int_0^{\epsilon} \epsilon^{3/2} f d\epsilon + \epsilon^{3/2} \int_{\epsilon}^{\infty} f \, d\epsilon + \frac{E^2}{E_0^2} \frac{\epsilon^3}{1 + \Omega^2 \epsilon^3}\right]. \tag{49}$$

When the normalized electron energy ϵ is large compared to 1 the coefficient γ, the (incomplete) number density, goes to 1; the coefficient β, the (incomplete) energy, also asymptotes to 1. For a maxwellian with average energy $3\epsilon_0/2$, $f \propto \exp(-\epsilon/\epsilon_0)$, where $\gamma\epsilon_0 = \beta$.

The distribution function has to satisfy a number of conditions. At the boundary $\epsilon \to \infty$ f and $\partial f/\partial\epsilon$ are zero, but there is no such condition at $\epsilon = 0$. Instead, there is the important condition that f remain positive, which is trivially satisfied, and the normalization condition, $\int_0^{\infty} \epsilon^{1/2} f \, d\epsilon = 1$. A second condition may follow from physical requirements, e.g. one may wish to have the energy loss in the inelastic collisions compensated exactly by an explicit energy source, such as the electric field.

A numerical solution is straightforward provided the equations can be linearized, i.e. a previously calculated distribution function is used to find the coefficients γ and β. This is a reasonable procedure because the coefficients are insensitive to the exact shape of the distribution. In doing this another requirement may be that the temperature of the plasma correspond to the temperature of the distribution that enters the coefficients. Finally, the solution can be iterated until convergence is obtained.

An interesting feature of the solution are the large changes in the tail, while the body remains the same. Now the question is, what do we want with this?

One especially interesting case occurs when the inelastic collision rate is large (compared to the electron-electron scattering rate) for a process at moderate low energy that in itself is not critical. The distribution function's tail will then be substantially affected, and the collision rate is suppressed at a higher energy where the interesting process takes place. Something similar should happen when all the inelastic processes are taken into account. Estimates along the same lines as presented here are possible, but will not be highlighted because they would be more believable with a numerical code, whose development is already sufficiently motivated.

6.5 ELECTRIC FIELD EFFECTS.

An equilibrium distribution in the absence of inelastic collisions, but with an electric and magnetic field is formally

$$h \sim \exp -\left[\int_0^{\xi} \frac{3\xi C(\xi) d\xi}{3\xi D(\xi) + 3(E/E_0)^2 \xi^6/(1 + \Omega\xi^6)}\right] \tag{50}$$

with the additional condition that the normalisation be maintained,

$$C(\infty) = \int_0^\infty d\xi\ \xi^2 h = 1. \tag{51}$$

For a weak electric field E the asymptotic forms of C and 3ξD are unity, and the distribution reduces to the equilibrium Maxwellian $h \sim \exp(-3\xi^2/2)$. When the magnetic field is large, such that $\Omega\xi^3 \ll 1$ over most of the interesting region, the electric field term becomes a constant,

$$3\xi(\frac{E}{E_0\Omega})^2 \times \frac{\xi^5}{\Omega^{-2}+\xi^6} \approx 3(\frac{E}{E_0\Omega})^2; \tag{52}$$

In this limit the term is small compared to unity, basically because anywhere away from the central region in the pinch $(v_0/v_D)^2 \ll 1$. Hence the electric field does not modify the denominator $3\xi D \sim 1$, and the electron distribution is basically thermal.

In contrast, along the pinch axis $\Omega = 0$, and the integrand in the exponent converges, showing that the present formulation is not rigorous in a runaway regime.

Even though the integral does not converge the expression can be a good approximation to the distribution function provided the integral is large compared to 1, i.e. the exponential factor is close to zero. Then the term $(E/E_0)^2$ in the denominator suggests an enhancement to the electron temperature.

In any case, it seems that effectively hot electron distributions can be generated with electric fields, but only along the pinch axis where the magnetic field vanishes. Let the boundary for this effect be $\omega_{ce}\tau_{ei} = 1$ $(\Omega = 1)$. In numerical units, this occurs at a radius r inside the pinch where

$$r(mm) = \frac{n(cm_3)}{3\times 10^{18}\ I(MA)\ Z\ T^{3/2}(eV)}, \tag{53}$$

assuming that the current density is constant over the pinch. Thus, this argument does not apply to the runin stage, but only to the stagnation stage of the pinch already collapsed on axis.

We must now ask if there is experimental evidence for tighter bright spots when Z is large. Riordan[31] compares the emission from pinches with different materials. These indeed show that tungsten has smaller bright spots than aluminum. intriguing. Further work might shed clearer light on such phenomena.

TABLE I. Symbol, edge and periphery.

	Symbol	edge	periphery
Current	I	2 MA	
Radius	r	1 mm	20 mm
Magnetic field	B	1000 T	50 T
Gyrofrequency	$\omega_c = eB/m$	$10^{14}/s$	5×10^{12}
gyroradius	r_e	$10^{-5}cm$	10^{-5} cm(?)
plasma frequency	ω_p	$10^{15}/s$	10^{12}/s(?)
Electron density	n_e	$10^{20}/cm^3$	$10^{14}/cm^3$(?)
Ion density	n_i	$10^{19}/cm^3$	$10^{13}/cm^3$(?)
Typical ionic charge	Z	10	10
ionic size	a_o/Z	$10^{-9}cm$	
Electron temperature	T_e	300 eV	10 keV (?)
Ion temperature	T_i	300 eV (?)	1 keV (?)
Debye length	λ_D	10^{-6}cm	3×10^{-5}cm
Plasma parameter	$n_e\lambda_D^3$	100	3
e-e collision time	τ_{ee}	1.5 ps	100μs(?)
e-i	$\tau_{ei} = \tau_{ee}/Z$	0.15 ps	10μs(?)
e-i energy exchange	$\tau_\epsilon = (M/m)\tau_{ei}$	30 ns	ms (?)
collisionality	$\omega_{ce}\tau_{ei}$	$30 \gg 1$	$10^7 \gg 1$(?)
ionization: Ar	energy 2 keV		
rate coefficient	$k =< \sigma v >$	$10^{-11}cm^3/s$	
inelastic collision time	τ_c	10 ns	
Charge/length	Ne	6 Coul/cm	
drift velocity	v_D	$3 \times 10^5 cm/s$	
drift distance in τ_c	Δx_c	$3 \times 10^{-3}cm$	

SECTION 7

LIST OF REFERENCES

1. N.R. Pereira and J. Davis, in preparation for Appl. Phys. Reviews.
2. S.L. Wong, C. Gilman, P Sincerny, and T Young, presented at the IEEE Intl. Conf. on Plasma Science (1982).
3. J.P. Apruseze and J. Davis, NRL Memorandum Report 5406 (1984).
4. F.L. Cochran,private communication.
5. F.S. Felber, Phys. Fluids **25** 643 (1982).
6. M.A. Liberman and A.L. Velikovich, preprint to be published in Nuclear Fusion.
7. e.g. R.W. Clark, R. Richardson, J. Brannon, M. Wilkinson, and J. Katzenstein, J. Appl. Phys. **53** 5552 (1982).
8. e.g. R.W. Clark, M. Gersten, J. Rauch, R. Richardson, and M. Wilkinson, J. Appl. Phys. **53** 4099 (1982).
9. B. Goplen, R.E. Clark, J. McDonald, and W.M. Bollen, Mission Research Corp. Report MRC-WDC-R-068 (1983).
10. e.g. R.H. Levy, Phys. Fluids **8**, 1288 (1965); R.J. Briggs, J.D. Daugherty and R.H. Levy, Phys. Fluids **13**,421 (1970); R. C. Davidson, **The theory of non-neutral plasmas**, (Benjamin, Reading, MA, 1974); R. C. Davidson, Phys. Fluids **27**, 1804 (1984).
11. e.g. M.V. Melander, N.J. Zabuski, and J.C. McWilliams, Phys. Fluids **30**, 2610 (1987).
12. M.S. di Capua, IEEE Trans. Plasma Science, **PS-11**, 205 (1983).
13. A. Ron, A. Mondelli and N. Rostoker, IEEE Trans. Plasma Science, **PS-1**, 85 (1973); R.V. Lovelace and E. Ott, Phys. Fluids **17**, 1263 (1974).
14. J. M. Creedon, J. Appl. Phys. **48**, 1070 (1977).
15. F. C. Young, private communication.
16. I.P.Shkarofsky, T.W. Johnston, and M.P. Bachynski, *The particle kinetics of plasmas*, Addison-Wesley, Reading, 1966.
17. T.H. Kho, preprint submitted to Phys. Rev **A**.
18. A.B. Langdon, Phys. Rev. Lett. **44**, 575 (1980).
19. R.S. Smith, Ph. D. Thesis, N. C. State University (1984).
20. R.F. Benjamin, J.S. Pearlman, E.Y. Chu, and J.C. Riordan, Appl. Phys. Lett. **39**, 848 (1981).
21. R. E. Terry, in preparation.
22. S.I. Braginskii, *Transport phenomena in plasmas*, in **Reviews of Plasma Physics**, Vol. I, Consultants Bureau, NY, 1965.
23. E.M. Epperlein, *The accuracy of Braginskii's transport coefficients for a Lorentz plasma*, J. Phys. D: Appl. Phys. **17** 1823 (1984).

24. V.E. Golant, A.P. Zhilinskii and I.E. Sakharov, *Fundamentals of Plasma Physics*. Wiley, NY 1980.
25. T.H. Kho, *Relaxation of a system of charged particles*, submitted to Phys. Rev **A**.
26. I.P.Shkarofsky, T.W. Johnston, and M.P. Bachynski, *The particle kinetics of plasmas*, Addison-Wesley, Reading, 1966.
27. L.G.H. Huxley and R.W. Crompton, *The drift and diffusion of electrons in gases*, Wiley, NY 1974.
28. A.B. Langdon, *Nonlinear inverse bremsstrahlung and heated electron distributions*, Phys. Rev. Lett. **44** 575 (1980).
29. R.Z. Sagdeev and A.A.Galeev, *Nonlinear plasma theory*, Benjamin, NY (1969).
30. D.L. Matthews, R.L. Kauffman, J.D. Kilkenny and R.W. Lee, *Electron energy distributions using the time-resolved free-bound spectra from coronal plasmas*, Appl. Phys. Lett. **44**, 586 (1984).
31. Riordan, J.C., Pearlman, J.S., Gersten, M., and Rauch, J.E., *Sub-Kilovolt X-ray Emission from Imploding Wire Plasmas*, AIP Conference proceedings, edited by D. Attwood and B. Henke (APS, New York), Vol. 75 (1981).

DISTRIBUTION LIST

DNA-TR-89-266

DEPARTMENT OF DEFENSE

ASSISTANT TO THE SECRETARY OF DEFENSE
ATTN: EXECUTIVE ASSISTANT

DEFENSE INTELLIGENCE AGENCY
ATTN: RTS-2B

DEFENSE NUCLEAR AGENCY
ATTN: RAAE
ATTN: RAEE
2 CYS ATTN: RAEV
4 CYS ATTN: TITL

DEFENSE NUCLEAR AGENCY
ATTN: TDNM
ATTN: TDTT
2 CYS ATTN: TDTT W SUMMA

DEFENSE TECHNICAL INFORMATION CENTER
2 CYS ATTN: DTIC/FDAB

THE JOINT STAFF
ATTN: J BUTTS

DEPARTMENT OF THE ARMY

HARRY DIAMOND LABORATORIES
ATTN: SLCHD-NW-RA
ATTN: SLCHD-NW-RS KERRIS
ATTN: SLCIS-IM-TL

U S ARMY MISSILE COMMAND/AMSMI-RD-CS-R
ATTN: AMSMI-RD-CS-R

U S ARMY NUCLEAR & CHEMICAL AGENCY
ATTN: MONA-NU

USA SURVIVABILITY MANAGMENT OFFICE
ATTN: SLCSM-SE J BRAND

DEPARTMENT OF THE NAVY

NAVAL RESEARCH LABORATORY
ATTN: CODE 2000 J BROWN
ATTN: CODE 4700 S OSSAKOW
ATTN: CODE 4720 J DAVIS
ATTN: CODE 4770 G COOPERSTEIN

NAVAL SURFACE WARFARE CENTER
ATTN: CODE R41

NAVAL SURFACE WARFARE CENTER
ATTN: CODE H-21

DEPARTMENT OF THE AIR FORCE

ASSISTANT CHIEF OF STAFF
ATTN: AFCSA/SASA W BARATTINO

SPACE DIVISION/CNCIV
ATTN: YNV

SPACE DIVISION/XR
ATTN: XR (PLANS)

SPACE DIVISION/YA
ATTN: YAR
ATTN: YAS

SPACE DIVISION/YE
ATTN: SD/CWNZ

WEAPONS LABORATORY
ATTN: WL/SUL

DEPARTMENT OF ENERGY

DEPARTMENT OF ENERGY
OFFICE OF MILITARY APPLICATIONS
ATTN: C B HILLAND, DP-243
ATTN: OFC OF INERT FUSION
ATTN: OFC OF INERT FUSION R SHRIEVER

LAWRENCE LIVERMORE NATIONAL LAB
ATTN: L-153
ATTN: L-545 J NUCKOLLS

LOS ALAMOS NATIONAL LABORATORY
ATTN: B259 J BROWNELL

SANDIA NATIONAL LABORATORIES
ATTN: DIV 9352 C DRUMM
ATTN: M J CLAUSER ORG 1201
ATTN: ORG 1230
ATTN: ORG 2312 D J ALLEN
ATTN: TECH LIB 3141

OTHER GOVERNMENT

CENTRAL INTELLIGENCE AGENCY
ATTN: OSWR/NED
ATTN: OSWR, J PINA

DEPARTMENT OF DEFENSE CONTRACTORS

ADVANCED RESEARCH & APPLICATIONS CORP
ATTN: R ARMISTEAD

AEROSPACE CORP
ATTN: LIBRARY ACQUISITION M1/199

BDM INTERNATIONAL INC
ATTN: E DORCHAK

BDM INTERNATIONAL INC
ATTN: L O HOEFT

BERKELEY RSCH ASSOCIATES, INC
2 CYS ATTN: E ALCARAZ
2 CYS ATTN: M PEREIRA

CALSPAN CORP/AEDC
ATTN: W G KIRBY

EOS TECHNOLOGIES, INC
ATTN: B GABBARD

GENERAL ELECTRIC CO
ATTN: H ODONNELL

JAYCOR
ATTN: E WENAAS

JAYCOR
ATTN: E WENAAS
ATTN: R SULLIVAN

KAMAN SCIENCES CORP
ATTN: D CALDWELL
ATTN: S FACE

KAMAN SCIENCES CORP
ATTN: DASIAC
ATTN: E CONRAD

KAMAN SCIENCES CORPORATION
ATTN: DASIAC

LOCKHEED MISSILES & SPACE CO, INC
ATTN: L CHASE

LOCKHEED MISSILES & SPACE CO, INC
ATTN: S TAIMUTY

MAXWELL LABS, INC
ATTN: A KOLB
ATTN: M MONTGOMERY

MCDONNELL DOUGLAS CORPORATION
ATTN: S SCHNEIDER

MISSION RESEARCH CORP
ATTN: C LONGMIRE

MISSION RESEARCH CORP, SAN DIEGO
ATTN: V VAN LINT

PACIFIC-SIERRA RESEARCH CORP
ATTN: H BRODE
ATTN: L SCHLESSINGER

PHYSICS INTERNATIONAL CO
ATTN: C GILMAN
ATTN: C STALLINGS
ATTN: G FRAZIER

PULSE SCIENCES, INC
ATTN: I D SMITH
ATTN: P W SPENCE
ATTN: S PUTNOM

R & D ASSOCIATES
ATTN: P TURCHI

RAND CORP
ATTN: B BENNETT

S-CUBED
ATTN: A WILSON
ATTN: J M WILKENFELD
ATTN: S L JURIST

SCIENCE APPLICATIONS INTL CORP
ATTN: W CHADSEY

SCIENCE APPLICATIONS INTL CORP
ATTN: K SITES

TRW INC
ATTN: TECH INFO CTR

TRW SPACE & DEFENSE SECTOR SPACE &
ATTN: D M LAYTON

FOREIGN

FOA 2
ATTN: B SJOHOLM

FOA 3
ATTN: T KARLSSON